AD-784 190

EXPERIMENTAL VERIFICATION OF SYSTEM
IDENTIFICATION

W. G. Flannelly, et al

Kaman Aerospace Corporation

Prepared for:

Army Air Mobility Research and
Development Laboratory

August 1974

| REPORT DOCUMENTATION PAGE | | READ INSTRUCTIONS BEFORE COMPLETING FORM |
|---|---|---|
| 1. REPORT NUMBER<br><br>USAAMRDL-TR-74-64 | 2. GOVT ACCESSION NO. | 3. RECIPIENT'S CATALOG NUMBER<br><br>AD 784190 |
| 4. TITLE (and Subtitle)<br><br>EXPERIMENTAL VERIFICATION OF SYSTEM IDENTIFICATION | | 5. TYPE OF REPORT & PERIOD COVERED<br><br>Final Report |
| | | 6. PERFORMING ORG REPORT NUMBER<br><br>Kaman Report R-1275 |
| 7. AUTHOR(s)<br><br>W. G. Flannelly<br>N. Giansante | | 8. CONTRACT OR GRANT NUMBER(s)<br><br>DAAJ02-73-C-0036 |
| 9. PERFORMING ORGANIZATION NAME AND ADDRESS<br><br>Kaman Aerospace Corporation<br>Old Windsor Road<br>Bloomfield, Connecticut 06002 | | 10. PROGRAM ELEMENT, PROJECT, TASK AREA & WORK UNIT NUMBERS<br><br>Project 1F162204A17002 |
| 11. CONTROLLING OFFICE NAME AND ADDRESS<br><br>Eustis Directorate, U. S. Army Air Mobility Research and Development Laboratory<br>Fort Eustis, Virginia 23604 | | 12. REPORT DATE<br><br>August 1974 |
| | | 13. NUMBER OF PAGES<br><br>95 |
| 14. MONITORING AGENCY NAME & ADDRESS(If different from Controlling Office) | | 15. SECURITY CLASS. (of this report)<br><br>Unclassified |
| | | 15a. DECLASSIFICATION/DOWNGRADING SCHEDULE |

16. DISTRIBUTION STATEMENT (of this Report)

Approved for public release; distribution unlimited.

17. DISTRIBUTION STATEMENT (of the abstract entered in Block 20, if different from Report)

18. SUPPLEMENTARY NOTES

19. KEY WORDS (Continue on reverse side if necessary and identify by block number)

| | |
|---|---|
| Identification | Structural properties |
| Mobility | Dynamics |
| Impedance | Vibration |
| Acceleration | |
| Frequency | |

20. ABSTRACT (Continue on reverse side if necessary and identify by block number)

Laboratory testing of system identification by single-point excitation showed correlation among the parameters identified by free-body shaking at two different points and theoretically derived parameters of the test specimen. Among the parameters investigated were the mass and stiffness matrices of five- and six-degree-of-freedom models and the structural damping coefficient of a continuous specimen. Experimentation demonstrated the identification of mathematical models having more degrees of freedom than modes in the measurements, a method of obtaining modal parameters by antiresonance theory, an engineering solution to the problem of imaginary antiresonances in Biot's Equation and Duncan's Equation for transfer impedances, a method of

DD FORM 1473 1 JAN 73     EDITION OF 1 NOV 65 IS OBSOLETE     Unclassified

Block 20. Abstract - continued.

obtaining static influence coefficients by free-body testing without assumption of a mass matrix, and a method of determining static structural test loads of helicopter maneuvers. Results indicate that iteration in system identification is not necessary for light damping and that one iterative method is divergent for damping.

The experimental results show that system identification can be effectively applied to continuous structures which are dynamically asymmetrical and nonuniform to determine lumped parameter mathematical models with testing over a limited range of frequencies.

# TABLE OF CONTENTS

1

## TABLE OF CONTENTS (Continued)

## Eustis Directorate Position Statement

The test structure to evaluate system identification by impedance techniques was an elastically uniform beam with three lumped masses asymmetrically placed on the beam. This structure was amenable to analysis by established procedures and was sufficiently complex to provide a good test of the impedance technique. The program was successful and verifies the use of impedance techniques for system identification of complex structures. Results of the program indicate that this system identification technique is satisfactory for further research, development, and testing on full-scale, complex, helicopter structures.

This report has been reviewed by this Directorate and is considered to be technically sound. The technical monitor for this contract was Mr. A. J. Gustafson, Technology Applications Division.

2

# LIST OF ILLUSTRATIONS

## LIST OF TABLES

# INTRODUCTION

## UNIFICATION OF TESTING AND ANALYSIS

System identification may be defined as methods of determining the parameters of a system from testing. In helicopter dynamics it generally refers to the determination of the inertial parameters, the elastic parameters, and the damping parameters of a structure (e.g., an engine, fuselage, rotor blade) directly from shake testing. System identification is not a replacement for a priori analytical methods but, rather, augments intuitively based analyses by closing the engineering loop between analytical engineering, which predicts effects, and test engineering, which measures these effects on the actual hardware.

Traditionally in helicopter engineering, structural dynamic testing served mainly to simply either confirm or deny what had been predicted by analysis. Our thinking tools in helicopter engineering, which we use in deciding how to improve our designs, have been principally based on conceptual idealizations of analytical form with little more benefit from actual testing than corroboration of predictions from our abstractions or, very often, evidence of mysteries beyond our capabilities of abstract formulation. Analysis is valuable in helicopter engineering only to the extent that it affects engineering decisions.

We can use system identification testing to provide information of decision-making value, obtained from the actual hardware, and to combine testing with analysis in a more unified engineering approach to the development of helicopter, and helicopter component, structures. Helicopters do not "fly off the drawing board". Most of the engineering is done, and most of the problems are solved, after a ship has been built. System identification will provide an analytic feedback from testing, badly needed, so that as successive new ships are built, more of the problems will be solved before the ship is built. In the shorter term, system identification will short-circuit much of the trial and error in the development of hardware helicopters, as opposed to paper helicopters, by extraction of analytical parameters from the helicopters themselves through testing.

7

The need for a more unified dynamics test and analysis
approach to all of aerospace structures and substructures
is widely proclaimed (e.g., References 1, 2, and 3) and the
helicopter is the most dynamically troubled of any flying
machine (Reference 4).

System identification is not a panacea for structural
dynamics problems. The logical extension of what are
called "Impedance Methods" to their most useful engineering
level, system identification is a synergistic combination of
what we can measure in the hardware with what we analytically
conceive of as idealizations of the hardware into a single
engineering system of rational decision making in the per-
fection of helicopters and their components.

## SYSTEM IDENTIFICATION - SOLUTION

Utilizing "impedance" test data, system identification
distills from shake testing the principal parameters of
analytical concern. The concern at present is in obtaining
elastic and inertial parameters of a helicopter structure
or substructure, primarily, and damping parameters,
secondarily, through testing. It is the first task of
system identification in helicopter work to separate the
elastic parameters from the inertial parameters and identify
each. We do this first in terms of what are called "measur-
ables", such as influence coefficients, which are independent
of the number of measurement stations. Mass information and
stiffness information which readily divide into "measurables"
through system identification cannot generally be obtained
in static testing either because of confounding of the
parameters, as in drop tests, or because of very small
displacements, as in deflection tests.

Having obtained "measurable" parameters through impedance
shake testing, the engineer then employs the methods of
system identification to obtain equations of motion of the
helicopter or its components as revealed by the testing
itself. The engineer can use these equations to predict
response to various loadings, to predict the dynamic effects
of identified subsystems, to predict the effects of changes
he can model in the structure, and to improve his a priori
intuitive modeling techniques. In any case, the equations and
parameters obtained from the structure itself will supplant
what we intuitively suppose to be parameters and equations
when we make engineering decisions about a helicopter. It
is the feedback to analysis from testing that is the most
valuable engineering part of system identification.

8

## SYSTEM IDENTIFICATION LABORATORY TESTING

To test the methods of system identification in a manner that
would allow comparisons to well established analytical pro-
cedures, it was decided to use a specimen of fairly ideal
analytic form. The fact that the specimen in the tests was
generally amenable to analysis had no influence, in itself,
on the ease with which the identifications could be made from
test data. It was further decided that the specimen in the
laboratory testing should be a continuous structure, as
opposed to a simple chain type structure, so that it would
not be a specimen with essentially only a few degrees of
freedom. An elastically uniform beam satisfied these con-
ditions, and a steel tubular beam was selected as the basic
form of the specimen. To eliminate dynamic symmetry and
uniformity, three lumped masses were asymmetrically placed
on the beam.

From the standpoint of system identification, the laboratory
specimen was therefore a continuous structure of an infinite
number of degrees of freedom which was dynamically asymmetric
and nonuniform. From the standpoint of intuitive analysis,
however, the specimen was simple enough for approximate
theoretical calculation of the parameters to be identified
so that the theoretical and identified parameters could be
compared.

The specimen was suspended to simulate free-body responses
because helicopters are generally shake tested, ground
resonance testing being the exception, suspended as free
bodies. To restrict the identification to a maximum of
six lumped parameters, it was specified that only five
accelerometers, plus the impedance head, could be used.

Comparison of system identification results to parameters
derived from theoretical analysis of the specimen was not
considered sufficient laboratory demonstration of the single-
point system identification theory, so it was required that
identifications be made independently from test data obtained
by shaking at two stations. The shaking stations selected
were 1/2 inch from one end of the specimen and 2-1/2 inches
from the opposite end of the specimen. This allowed a
three-way comparison of results among theoretical analysis
and two independent identifications.

9

Correlation among the three methods of obtaining parameters was done for matrices of a five-degree-of-freedom model covering five modes and a six-degree-of-freedom model covering five modes, the latter being a truncated model. Correlation was obtained on modal accelerations (normal modes and generalized masses), inertial coefficient matrices, mass matrices, free-body influence coefficient matrices, stiffness matrices, and static influence coefficient matrices. The structural damping coefficient was determined for both the five-degree-of-freedom model and the six-degree-of-freedom model. A method of identifying static structural test loads and deflections was demonstrated for the six-degree-of-freedom model using five modes and using four modes.

# DISCUSSION OF CONCEPTS AND METHODS

## MOBILITY

### Mobility and Impedance

At any frequency, $\omega$, the equations of motion of a linear structure with Soroka structural damping are

$$[K - \omega^2 M + igK]\{y\} = \{f\} \tag{1}$$

We abbreviate the expression by referring to the terms in the matrix as the "displacement impedance", Z (Reference 5).

$$[Z]\{y\} = \{f\} \tag{2}$$

We denote the "acceleration impedance" as $\ddot{Z}$ and define it as the matrix coefficient of the acceleration in the equation giving the forces. For reasons to be explained later, we will be working with accelerations, rather than velocities or displacements.

$$[\ddot{Z}]\{\ddot{y}\} = \{f\} \tag{3}$$

Note that $\ddot{Z}$ is not the second derivative of Z with respect to time, which is self-evident in the context in which it is used, and we adopt this slight abuse of mathematical nomenclature because of the much needed simplification it affords in impedance terminology by the very obvious meaning it has to helicopter engineers.

From Equation (3) we see that the accelerations are given by

$$\{\ddot{y}\} = [\ddot{Z}]^{-1}\{f\} \equiv [\ddot{Y}]\{f\} \tag{4}$$

in which the inverse of $\ddot{Z}$, the acceleration impedance, is called the "acceleration mobility", $\ddot{Y}$. Unless otherwise specified, our use of the term "mobility" is to be taken to mean "acceleration mobility".

As seen from the matrix expressions, impedance and mobility are properly partial derivatives. Acceleration impedance is the partial derivative of force with respect to acceleration. Acceleration mobility is the partial derivative of acceleration with respect to force. The j-th acceleration, as seen from Equation (4), can be written as

11

$$\frac{\partial \ddot{y}_j}{\partial f_1} f_1 + \frac{\partial \ddot{y}_j}{\partial f_2} f_2 + \frac{\partial \ddot{y}_j}{\partial f_3} f_3 + \ldots + \frac{\partial \ddot{y}_j}{\partial f_n} f_n = \ddot{y}_j \qquad (5)$$

or

$$\ddot{Y}_{j1} f_1 + \ddot{Y}_{j2} f_2 + \ddot{Y}_{j3} f_3 + \ldots + \ddot{Y}_{jn} f_n = \ddot{y}_j \qquad (6)$$

If we apply one and only one force, say at station k, then we see from Equation (6) that

$$\ddot{Y}_{jk} = \ddot{y}_j / f_k \qquad (7)$$

In other words, mobility becomes simply a ratio of acceleration to force when only one external force is applied. With an external force at k and only at k, we can measure all mobilities over j: $\ddot{Y}_{1k}$, $\ddot{Y}_{2k}$, $\ddot{Y}_{3k}$, etc., for as many or as few accelerometer stations j as we wish.

In a continuous structure we cannot measure the impedance $\ddot{Z}_{jk}$. This would require holding all the accelerations to zero but one and "all" the accelerations are infinite.

## Measurables and Abstractions

Suppose, now, that we ignore the "infinity minus one" problem by considering only a finite number of acceleration stations, say n. Further suppose that we found a practical method of holding n-1 accelerations to zero. Then we could measure any impedance $Z_{jk}$ for n stations. But if we considered N stations where $N \neq n$, then the value of $Z_{jk}$ for N stations would be different from the value of $Z_{jk}$ for n stations. We see, therefore, that the value of an impedance is a function of the number of stations chosen and is an abstraction wholly dependent on the analyst's intuitive simplification of a continuous structure to one of an arbitrary number of lumped coordinates.

This leads us necessarily into the concepts of "measurables" and "abstractions" which are covered in Reference 6. Impedance is not a measurable quantity because it is not a property of a continuous structure but, rather, depends on the number of coordinates chosen at the whim of the analyst. Mobility, to

12

the contrary, is a measurable quantity, a property of the structure at any frequency, and is completely independent of the number of coordinates the analyst wishes to consider.

Similarly, as shown in Reference 6, terms in the inverse of the mass matrix and terms in the inverse of the stiffness matrix (the influence coefficients) are measurable properties of the structure while elements of the mass and stiffness matrices are intuitive abstractions dependent on arbitrary choices of the analyst.

It is therefore quite obvious that the magnitudes of individual terms in the mass and stiffness matrices of a mathematical model of a continuous structure are not, in themselves, of informational value in engineering since a given term in, say, the stiffness matrix of a 100 x 100 is of quite different value than the same term in a 99 x 99 matrix of the same coordinates but one. This is not to say, continuing the example, that the stiffness matrix is not useful; it is not only useful but extremely important. The individual values of the elements in the stiffness matrix are not meaningful but the individual values of the elements in the inverse of the stiffness matrix are very meaningful.

In general, it is the inverse of the matrices to which the analysts are most accustomed which are natural properties of a structure, i.e., "measurables", and we deal with the abstract inverses of these measurables solely as mathematical tools. Some methods of using these abstract tools to practical purposes are covered in an appendix.

It is of prime importance in helicopter engineering to recognize that while mathematical "laws" bound the logic of our contemplation of the helicopter, the helicopter itself is a natural thing performing in a real world not fully described by the mathematics of which any of us are capable. The object of system identification is to make the mathematical methods with which we are familiar in the industry more capable of dealing with the facts of real helicopters, which we can measure.

## Modal Acceleration and Mobility

Let $\phi_{ji}$ be the j-th element of the i-th normal mode, $\phi_{ki}$ be the k-th element of the i-th normal mode and $M_i^*$ be the "generalized mass" of the i-th normal mode given by

$M_i^* = \{\phi\}_i^T [m] \{\phi\}_i$ where $[m]$ is the infinite ordered mass matrix of the structure. Then the jk-th modal acceleration of the i-th mode is defined as

$$A_{jki} = \frac{\phi_{ji}\phi_{ki}}{\{\phi\}_i^T [m] \{\phi\}_i} \qquad (8)$$

The response of an accelerometer at j for a force at k, in an undamped single-degree-of-freedom system, the acceleration mobility approaches the modal acceleration, $A_{jk}$, at forcing frequencies far above the natural frequency. In a multi-degree-of-freedom system, the acceleration mobility at frequencies far above the natural frequencies approaches the sum of the modal accelerations,

$$\sum_{i=1}^{n} A_{jki}.$$

The i-th modal acceleration of the j-th degree of freedom for a force at k is seen to be the frequency-independent measure of the contribution of the i-th mode to the acceleration at j for a force at k. In an undamped system of n modes, the acceleration mobility (for force at K) at any frequency $\omega$ is given by

$$\ddot{Y}_{jk\omega} = - \sum_{i=1}^{n} A_{jki} \frac{\omega^2/\Omega_i^2}{1 - \omega^2/\Omega_i^2} \qquad (9)$$

Similarly, in a system with Soroka structural damping, g, the real acceleration mobility is

$$\ddot{Y}^R_{jk\omega} = - \sum_{i=1}^{n} A_{jki} \; \frac{\omega^2}{\Omega_i^2} \; \frac{1 - \omega^2/\Omega_i^2}{(1 - \omega^2/\Omega_i^2)^2 + g_i^2} \qquad (10)$$

and the imaginary acceleration mobility is

$$\ddot{Y}^I_{jk\omega} = \sum_{i=1}^{N} A_{jki} \; \frac{\omega^2}{\Omega_i^2} \; \frac{g_i}{(1 - \frac{\omega^2}{\Omega_i^2})^2 + g_i^2} \qquad (11)$$

### Rigid-Body Acceleration Coefficient

In an unrestrained system we have up to six, say Z, "rigid body" degrees of freedom. This means we have Z natural frequencies which are zero. Setting the first Z natural frequencies to zero in Equation (10), we write

$$\ddot{Y}^R_{jk\omega} = \sum_{i=1}^{z} A_{jki} - \sum_{i=Z+1}^{N} A_{jki} \; \frac{\omega^2}{\Omega_i^2} \left( \frac{1 - \omega^2/\Omega_i^2}{(1 - \frac{\omega}{\Omega_i^2})^2 + g_i^2} \right) \qquad (12)$$

(Reference 7). The first term is, of course, a rigid-body property which we call the rigid-body acceleration coefficient (RAC) and denote it as $E_{jk}$. At zero forcing frequency the real acceleration mobility is equal to the rigid-body acceleration coefficient.

$$\ddot{Y}^R_{jk} = E_{jk} \text{ at } \omega = 0. \qquad (13)$$

The RAC, $E_{jk}$, is the acceleration along coordinate j (the accelerometer at j) for a steady force at k as the helicopter hurtles into space. If the force were a. the center of gravity the RAC would be the same value for every point on the ship, but when the force is not at the center of gravity the ship is rotating as well as translating and the RACs are different for different points. The RAC is easily calculated from helicopter weights data. If, for example, the ship has a total mass M, roll inertia $I_x$ and yaw inertia $I_y$, then lateral (y-direction) acceleration at j for a

lateral force at k is given by

$$E_{jk} = \frac{1}{M} + \frac{Z_j Z_k}{I_x} + \frac{X_j X_k}{I_y} \qquad (14)$$

where Z and X represent, as subscripted, distances from the
center of gravity to the accelerometer at j and the force at
k or vice versa. Equation (14) assumes principal axes. In
Appendix B we derive the general expression for the RAC for
principal or nonprincipal axes and all directions. The RAC
for the test specimen are presented in the following matrix
for stations 0.5, 6, 25, 35.5, 61, and 72.5 inches.

$$\begin{bmatrix}
53.856 & & & & \text{Symmetric} & \\
48.166 & 43.346 & & & & \\
28.51 & 26.696 & 20.429 & & & \\
17.647 & 17.494 & 16.966 & 16.674 & & \\
-8.733 & -4.852 & 8.555 & 15.964 & 33.958 & \\
-20.63 & -14.93 & 4.762 & 15.644 & 42.073 & 53.992
\end{bmatrix}$$

Suppose now that we specify a maneuver by hub forces h, hub
moments M and tail rotor thrust t. The steady accelerations
at the flight deck are then given by

$$\begin{bmatrix}
E_{xh} & E_{xM} & E_{xt} \\
E_{yh} & E_{yM} & E_{yt} \\
E_{zh} & E_{zM} & E_{zt}
\end{bmatrix}
\begin{Bmatrix} h \\ M \\ t \end{Bmatrix} =
\begin{Bmatrix} \ddot{x} \\ \ddot{y} \\ \ddot{z} \end{Bmatrix} \qquad (15)$$

or

$$[E]\{f\} = \{\ddot{q}\} \qquad (16)$$

Conversely, we can specify as many maneuver g-loadings, $\ddot{q}$,
as there are trim forces and moments and obtain the trim
forces and moments by

$$\{f\} = [E]^{-1}\{\ddot{q}\} \qquad (17)$$

16

Using antiresonance theory, which is discussed later, we see that the acceleration mobility at any frequency, which is a nonrigid response of the helicopter, can be obtained by multiplying the rigid body acceleration coefficient by a factor. This factor is a function of frequency only and involves the forcing frequency, the natural frequencies, and the antiresonant frequencies. See Figure 1.
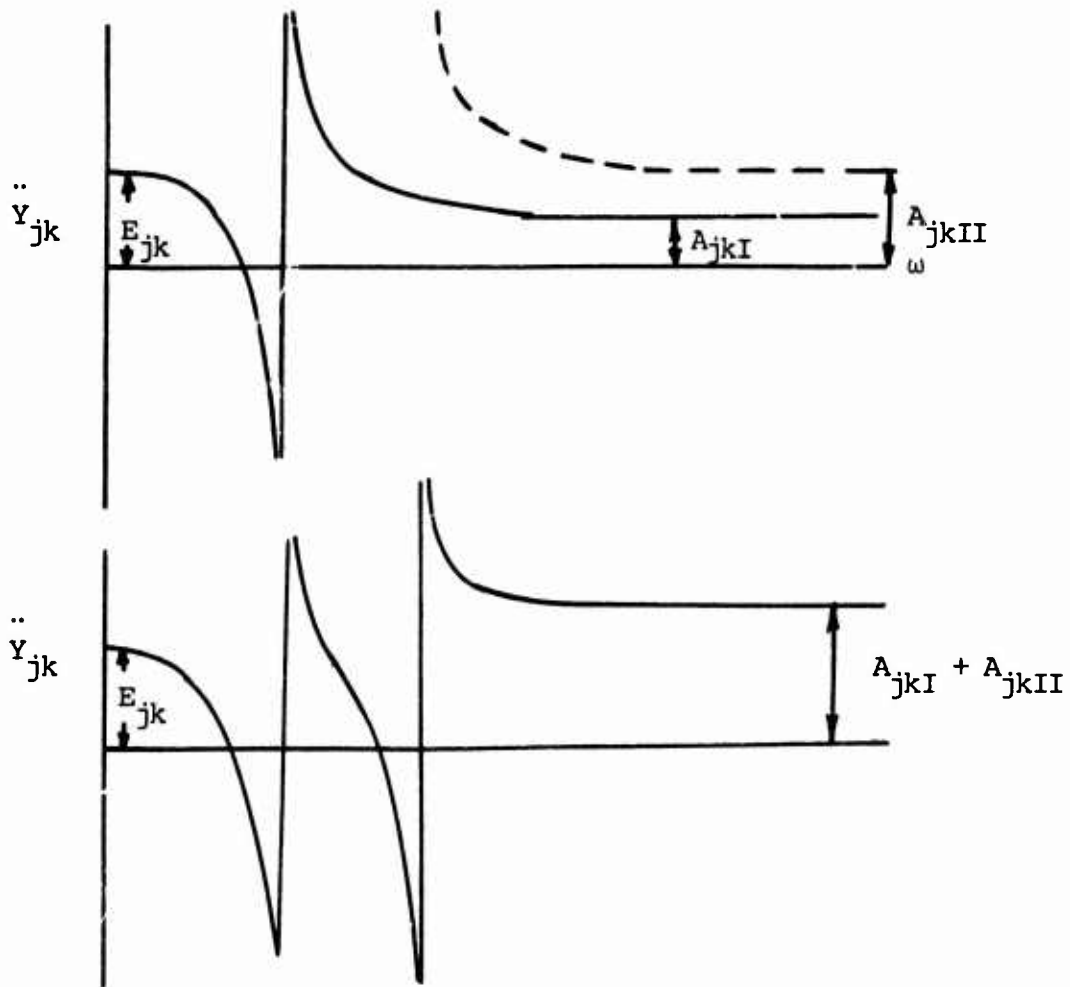


Figure 1. Mobility Versus Frequency.

## Free-Body Influence Coefficient

Now let us convert Equation (12) to displacement mobility by dividing through by minus the forcing frequency squared

$$Y^R_{jk\omega} = -\frac{E_{jk}}{\omega^2} + \sum_{i=Z+1}^{N} \frac{A_{jki}}{\Omega_i^2} \frac{1 - \omega^2/\Omega_i^2}{(1 - \omega^2/\Omega_i^2)^2 + g_i^2} \qquad (18)$$

With zero damping, this becomes

$$Y^R_{jk\omega} = -\frac{E_{jk}}{\omega^2} + \sum_{i=Z+1}^{N} \frac{A_{jki}}{\Omega_i^2} \frac{1}{1 - \omega^2/\Omega_i^2} \qquad (19)$$

If we let the forcing frequency go to zero in Equation (19) we would have the deflection at j due to a force at k but, because our system is unrestrained, we end up with an indeterminancy because of the first term involving the RAC. In other words, the static influence coefficients of a free body are infinite. But the second term is finite at zero frequency. To avoid confusion at the outset, we will call this second term the free-body influence coefficient, $C^E_{jk}$.

$$C^E_{jk} = \sum_{i=Z+1}^{N} \frac{A_{jki}}{\Omega_i^2} \qquad (20)$$

The physical meaning of the free body influence coefficient is quite simple. When the free body is hurtling into space at constant acceleration under a force at k, the body is deformed. The number of inches j is displaced, relative to inertial axes of body, per pound of force at k is the free-body influence coefficient, $C^E_{jk}$.

In a maneuver under forces and moments, f, wherever applied, the <u>deflections</u> of the helicopter structure, q, relative to the inertial axes through the center of gravity are given by

$$\{q\} = [C^E]\{f\} \qquad (21)$$

These deflections, and therefore the free-body influence coefficients, have less intrinsic engineering value than their value as engineering tools in obtaining such quantities as the purely elastic static influence coefficients of an

arbitrarily restrained free body, which will be discussed later. Note that the free-body influence coefficient is a static property of the structure but not purely an elastic property because it is a function of both the elastic and inertial properties.

We observe, without presenting proof, since it is not germane to the report, that the free-body influence coefficient is a function only of the RAC and the nonzero antiresonant and resonant frequencies.

$$C_{jk}^{E} = E_{jk} \left[ \sum_{i=Z+1}^{N} \frac{1}{a_{jki}^{2}} - \sum_{i=Z+1}^{N} \frac{1}{\Omega_{i}^{2}} \right]$$   (22)

## Three Parameters

In helicopter dynamics we deal with linear systems in which normal modes exist (Reference 5). To determine the physical parameters of a structure, there are three things we need to determine from shake tests: the natural frequencies, the modal accelerations, and the damping coefficients. Natural frequencies are readily determined mode-by-mode from the plots themselves. The damping coefficients are of secondary importance to the structural elastic and inertial properties of a helicopter and may be estimated mode-by-mode either from the mobility plots directly or, with more useful accuracy, evaluated in conjunction with the determination of the modal accelerations.

Modal accelerations are not obvious from the plots alone and cannot be determined for any one mode without consideration of other modes. They can, however, be determined for the response of any one accelerometer, given a shaking station, without considering any other accelerometer. Modal acceleration is the most difficult of the three parameters to determine from a shake test but several methods are available. Among the methods used in this contract we will present a new one, based on antiresonance theory, which is so simple that it does not require a computer but can be done by hand calculation.

Modal acceleration is introduced as a simplification of ambiguous and confusing mathematical terms such as "generalized mass" or "element of the orthogonal mode", the values of each of which depend on arbitrary "normalization" that makes them meaningless as independent measurable quantities. The value of the modal acceleration

19

for the i-th mode of an accelerometer at j for a force at k
is a physical quantity containing in itself, and indepen-
dently in itself, all the information of the jk response
in the i-th mode that several other pairs of definitions
encompass.  A term involving nomenclature such as "effective
mass", "apparent mass" or "modal mass" would suffice except
that their use would encumber specification of what is meas-
ured and there are so many different definitions of these
terms that what they have most in common is confusion.

## Natural Frequencies From Mobility Plots

The natural frequencies of consequence are accurately
approximated by a peculiar and easily identified shape of
the real acceleration mobility plots, as shown in Figure 2,
which generally crosses zero.
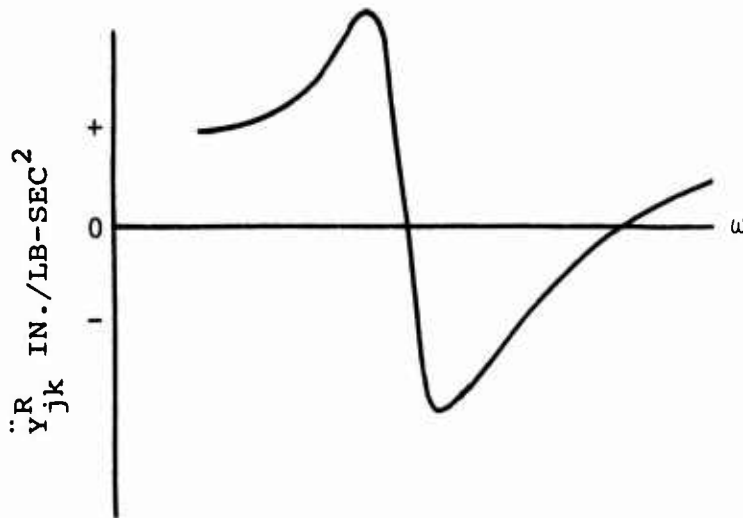


Figure 2.  Natural Frequency and Antiresonance.

The natural frequencies are distinguished from antiresonances
in three ways: (1) There is a peak immediately above and
below the real mobility of steep slope indicating a natural
frequency; antiresonant crossovers are not straddled by peaks.
(2) The natural frequencies are the same for every accelerom-
eter; antiresonant crossover frequencies are not the same
for every accelerometer. (3) The imaginary acceleration
mobility peaks at approximately the natural frequency, but
does not at an antiresonance.

In general, the mobility will cross zero at a natural
frequency, but in some cases, due to damping, the curve
will not cross zero but appear as shown in Figure 3. The
characteristic shape of the curve at a natural frequency
is retained, however, and comparisons with the imaginary
mobility for the accelerometer in question and with the real
and imaginary curves for the other accelerometers will re-
solve any practical possibility of doubt of the occurrence
of a natural frequency.
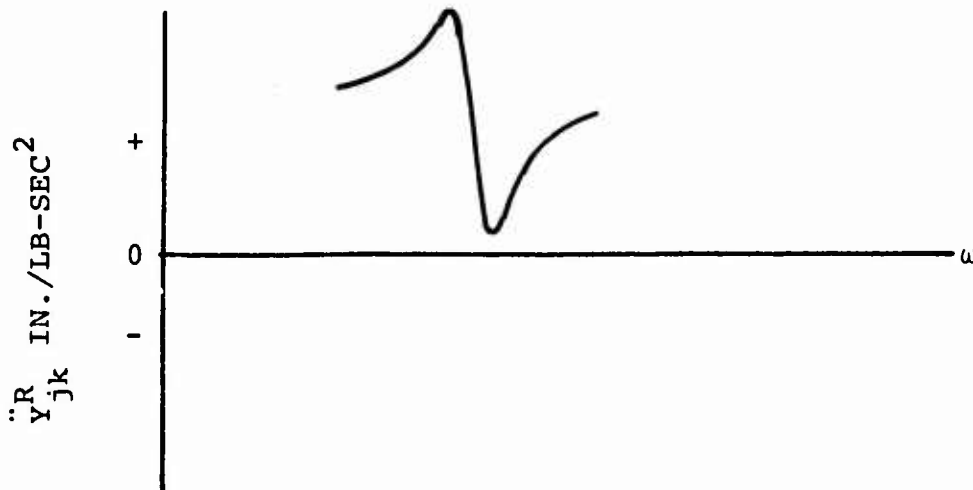


Figure 3.  Mobility May Not Cross Zero
at a Natural Frequency.

Peaks in the imaginary acceleration mobility plots and the characteristic steep between-peaks slope of the real acceleration mobility in a damped system indicate the "approximate" natural frequency. As shown in the classic paper of Kennedy and Pancu (Reference 8), the frequency at which the real acceleration mobility has a maximum rate of change with frequency is the best approximation to the "true" natural frequency, defined as the resonant condition of the system if the damping were completely removed. With the relatively low levels of damping characteristic of aerospace structures and the fact that the lower modes are of most importance in helicopter dynamics, the differences between the "approximate" natural frequencies revealed by the real acceleration mobility and the "true" natural frequencies (which would occur with the damping removed) are such small differences that the distinction is academic. The academic nature of the distinction in helicopter structural dynamics is further highlighted by the fact that, as was found in this work and other work by the authors, the identified elastic and inertial properties of a structure with typical semi-monocoque level Soroka damping are practically the same whether or not damping is included.

Immediately connected with the question of natural frequencies is that of determining the difference between a "major" or a "minor" mode. The latter is sometimes called, in a practical if mathematically imprecise way, a "local" mode. This will be dealt with in another section.

The method of determining natural frequencies given by Kennedy and Pancu 33 years ago remains the most practical method for aerospace structures and has been used by various people, including the authors, in helicopter work for 15 years when real and imaginary type data could be obtained, usually with rotary shakers. With the increasing utilization of modern impedance measurement equipment, it is possible to use the Kennedy-Pancu Principle for natural frequencies without the classic Kennedy-Pancu Plot, which in a complex structure is not practical for other than natural frequency determination, and with excitation from electromagnetic shakers instead of the less flexible counter-rotating rotary shakers.

## Modal Accelerations and Damping by Antiresonance Theory

Using a new equation of antiresonance theory, the engineer can determine modal accelerations of a lightly damped system with only a slide rule or "shirt pocket" calculator. This technique has the advantage of allowing rapid on-site checking of test data whether or not a computer terminal is immediately available. Because the modal acceleration is related to rigid body properties and the test data by one simple algebraic equation, many of the physical implications of the test parameters and numerical sensitivity of the calculation are obvious by inspection of the antiresonance equation. These cannot be found by inspection when, as with other methods of comparable accuracy, a matrix inversion is involved.

In a freely suspended system, the modal acceleration of the M-th mode for a driving point is given by:

$$A_{jj_M} = - E_{jj} \frac{\displaystyle\prod_{i=Z+1}^{N} (1 - \frac{\Omega_M^2}{a_{jj_i}^2})}{\displaystyle\prod_{\substack{m \neq M \\ m=Z+1}}^{N} (1 - \Omega_M^2/\Omega_m^2)} \qquad (23)$$

where $E_{jk}$ is a rigid body property (depending only on gross weight, c.g. location and inertias) the value of which is accurately known before any helicopter structure or major component is built. For transfer measurements (i.e., the response of an accelerometer to a force at some other station) some of the antiresonance frequencies may be imaginary, in which case testing will not reveal as many antiresonances as natural frequencies which are required in Equation (23). This problem is easily solved by shifting the zero mobility axis to create pseudo-antiresonances as many in number as natural frequencies. We do this by drawing a horizontal line at some mobility K through the mobility test plot so that the line crosses the test plot at as many frequencies as there are natural frequencies. The frequencies at which this line intersects the mobility are the pseudo-antiresonant frequencies, a, in Equation (24).

$$A_{jkM} = -(E_{jk} - K) \frac{\displaystyle\prod_{i=Z+1}^{N}(1 - \Omega_M^2/a_{jki}^2)}{\displaystyle\prod_{\substack{m \neq M \\ m=Z+1}}^{N}(1 - \Omega_M^2/\Omega_m^2)} \qquad (24)$$

Equation (24), and the technique used therein applied to similar equations, solves the imaginary antiresonance problem (References 9, 10, and 11) which emerged in 1940.
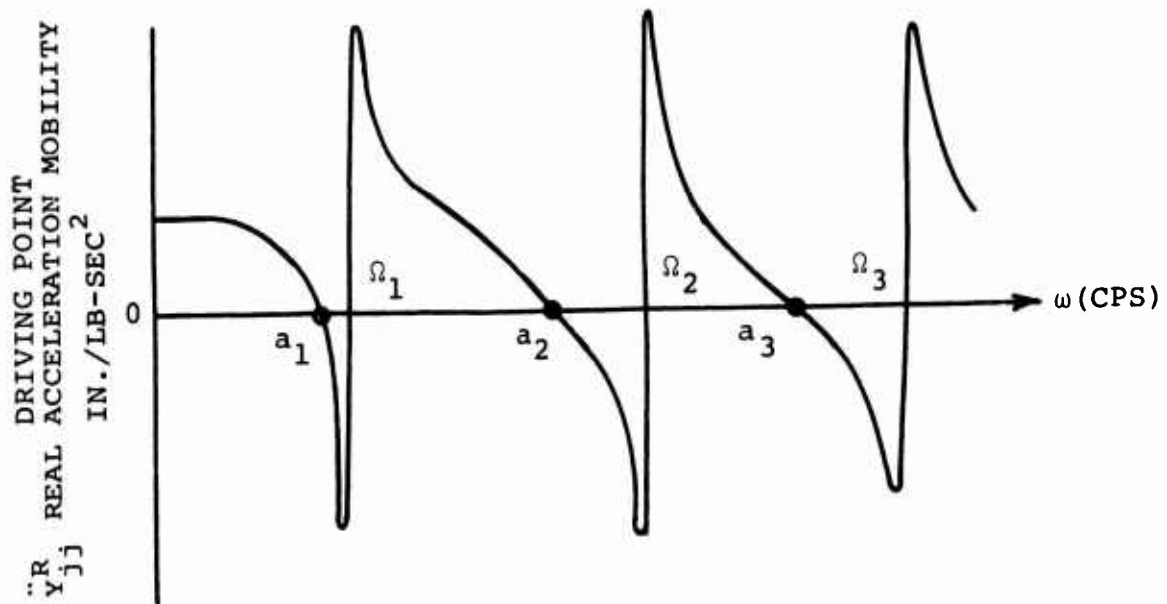


Figure 4.  Driving Point Mobility.
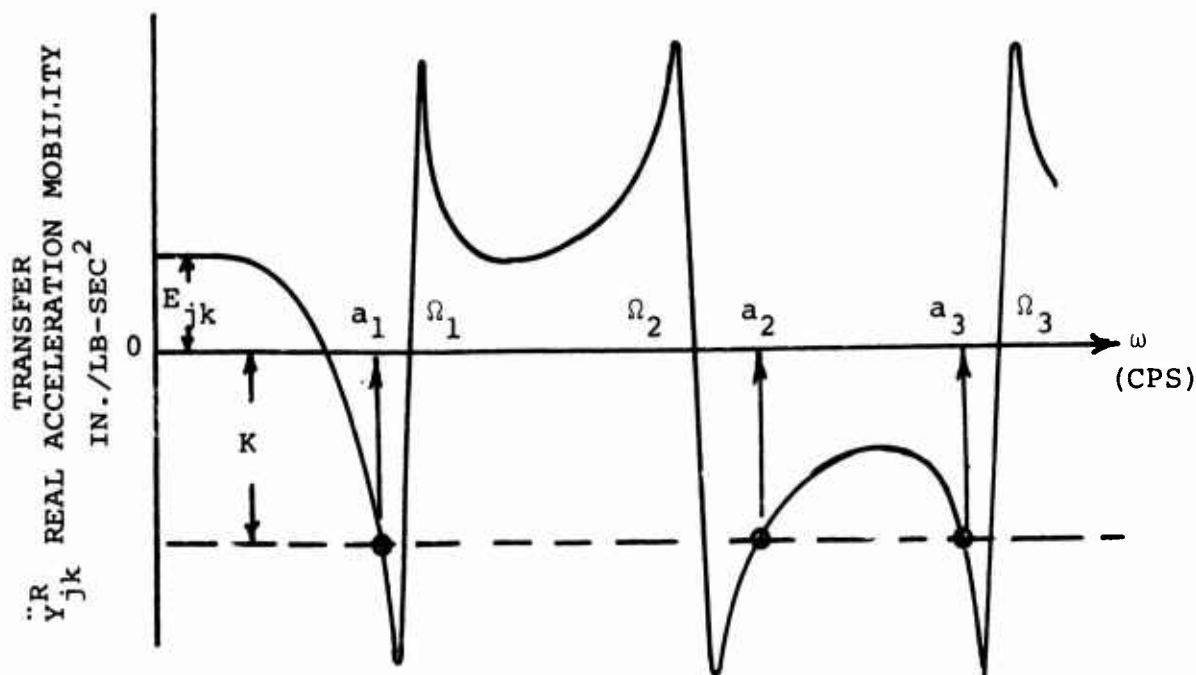
Figure 5.   Transfer Mobility.

The complex acceleration mobility is given by:

$$\ddot{Y}_{jk\omega}^{R} + i\, \ddot{Y}_{jk\omega}^{I} = E_{jk} \frac{\displaystyle\prod_{i=Z+1}^{N} (1 - \omega^2/a_{jki}^{\,2} + ig)}{\displaystyle\prod_{i=Z+1}^{N} (1 - \omega^2/\Omega_{i}^{\,2} + ig)} \qquad (25)$$

and for pseudo-antiresonances this may be written:

$$\ddot{Y}_{jk\omega}^{R} + K + i\, \ddot{Y}_{jk\omega}^{I} = (E_{jk} + K) \frac{\displaystyle\prod_{i=Z+1}^{N} (1 - \omega^2/a_{jki}^{\,2} + ig)}{\displaystyle\prod_{i=Z+1}^{N} (1 - \omega^2/\Omega_{i}^{\,2} + ig)}$$

$$(26)$$

At any pseudo-antiresonance, $\omega = a_{jkm}$, $\ddot{Y}^R_{jk\omega} + K = 0$ and Equation (26) becomes

$$i\,\ddot{Y}^I_{jkam} = ig(E_{jk} + K)\;\frac{\displaystyle\prod_{\substack{i=Z+1 \\ i\neq m}}^{N}\left(1 - \frac{a_{jkm}^2}{a_{jki}^2} + ig\right)}{\displaystyle\prod_{i=Z+1}^{N}\left(1 - \frac{a_{jki}^2}{\Omega_i^2} + ig\right)} \tag{27}$$

The damping coefficient is then seen to be approximated by

$$g \cong \frac{\ddot{Y}^I_{jkam}}{E_{jk} + K}\;\frac{\displaystyle\prod_{i=Z+1}^{N}\left(1 - \frac{a_{jki}^2}{\Omega_i^2}\right)}{\displaystyle\prod_{\substack{i\neq m \\ i=Z+1}}^{N}\left(1 - \frac{a_{jkm}^2}{a_{jki}^2}\right)} \tag{28}$$

## Modal Acceleration and Damping by Pseudoinverse Iteration of One Component

The derivation of psuedoinverse iteration is given in Reference 5. With very lightly damped systems, we prefer to work with the real acceleration mobility instead of the imaginary mobility because the imaginary mobility is difficult to accurately measure when the damping is very small. In using the real acceleration mobility we must remember that, different from the situation using the imaginary, we must include all the lower modes. In other respects, the process is the same using either real or imaginary mobilities.

For J accelerometers, P forcing frequencies and N modes, the equation to be solved is Equation (29).

$$[\ddot{Y}^R_{j(k)\omega} - E_{j(k)}] = [A_{j(k)i}][S_{i\omega}] + [R_{j\omega}] \tag{29}$$

$$\text{JxP} \qquad\qquad \text{JxN} \quad \text{NxP} \qquad \text{JxP}$$

$$S_{i\omega} = - \frac{\omega^2}{\Omega_i^2} \frac{1 - \omega^2/\Omega_i^2}{(1 - \frac{\omega^2}{\Omega_i^2})^2 + g_i^2} \qquad (30)$$

R is the matrix of residuals to be minimized.  When the number of forcing frequencies is equal to or greater than the number of modes, we calculate the S matrix ignoring damping and obtain A from Equation (31).

$$[A_{j(k)i}^{(1)}] = [Y_{j(k)\omega}^R - E_{j(k)}][S_{i\omega}^{(0)}]^+ \qquad (31)$$

where

$$[S_{i\omega}^{(0)}]^+ \equiv [S_{i\omega}^{(0)}]^T ([S_{i\omega}^{(0)}][S_{i\omega}^{(0)}]^T)^{-1} \qquad (32)$$

We may now take the A matrix given by Equation (31) as a first approximation and obtain a new S matrix.

$$[S_{i\omega}^{(1)}] = [A_{j(k)i}^{(1)}]^+ [\ddot{Y}_{j(k)\omega}^R - E_{j(k)}] \qquad (33)$$

where

$$[A_{j(k)i}]^+ \equiv ([A_{j(k)i}]^T [A_{j(k)i}]^{-1} [A_{j(k)i}]^T \qquad (34)$$

The process becomes an iteration, as shown in Reference 5, converging on the A matrix which minimizes the Euclidian norm of the residuals.

$$[A_{j(k)i}^{(2)}] = [\ddot{Y}_{j(k)\omega}^R - E_{j(k)}][S_{i\omega}^{(1)}] \qquad (35)$$

$$[S_{i\omega}^{(2)}] = [A_{j(k)i}^{(2)}]^+ [\ddot{Y}_{j(k)\omega}^R - E_{j(k)}] \qquad (36)$$

27

And the process is continued until the n+1 approximation to A is essentially the same as the n-th approximation. Using the elements of the converged S matrix and the elements of the initial S matrix, calculated without damping, we can solve for the structural damping coefficient, g.

This method of obtaining modal accelerations is most suitable when there are a large number of accelerometers being used in the test. The mobility data may be automatically sampled over all accelerometers at given frequencies.

Modal Acceleration and Damping From Iteration Using the Imaginary Mobility and Pseudoinverse of the Real

If we take one row of Equation (29), we have an expression for the jk-th mobility at different forcing frequencies in which there is a residual vector, R, when there are more forcing frequencies than modes in the equation.

$$\{\ddot{Y}_{(jk)\omega}\} = [S_{\omega i}]\{A_{(jk)i}\} + \{R_{(jk)\omega}\} \tag{37}$$

Performing the first step of the iteration of the previous section, as shown by Equation (31), to obtain the modal accelerations for the minimum Euclidian length of the residual vector.

$$\{A_{(jk)i}\} = [S_{\omega i}]^{+}\{\ddot{Y}^{R}_{(jk)\omega}\} \tag{38}$$

If the S matrix is square (i.e., if there are as many forcing frequencies as modes in the expression) and if the real acceleration mobilities are of equal value, then the modal accelerations obtained from Equation (38) are exactly those obtained by antiresonance theory from Equation (24). Equation (38) allows the engineer more flexibility in choosing mobility points and manipulating this data than does the antiresonance theory equation. It requires a computer for practical employment but this is not a serious drawback in many instances where time-sharing terminals can be used on-site. On the other hand, Equation (38) does not describe the physics of the situation as does Equation (24) relating the resonances and antiresonances to the modal parameters.

We may take the calculation of Equation (38) as a first approximation of the modal accelerations with the S matrix formed by assuming the damping to be zero. Noting that the imaginary acceleration mobility is given by

28

$$\{\ddot{Y}^{I}_{(jk)\omega}\} = [S^{I}_{\omega i}]\{g_{i}A_{(jk)i}\} \tag{39}$$

where

$$S^{I}_{\omega i} = g_{i} \tag{40}$$

We can solve Equation (39) for the product of the damping and modal accelerations as follows.

$$\{g_{i}A_{(jk)i}\} = [S^{I}_{\omega i}]^{+}\{\ddot{Y}^{I}_{(jk)\omega}\} \tag{41}$$

Between Equations (38) and (41) we can solve for the structural damping coefficient, $g_{i}$, for each mode and construct a new S matrix. Then we can solve Equation (38) again, using this new S matrix, for a better approximation of the modal accelerations, and continue the processes until the modal accelerations and structural damping coefficients have converged. Except that we input the rigid-body acceleration coefficient, $E_{jk}$, as known data, this is the process described by Klostermann in Reference 12, which differs from Stahle's approach (Reference 13) in the use of the pseudoinverse.

## Other Methods of Determining Damping

As seen in Figure 3, the real mobility has a maximum just below the natural frequency and a minimum just above it. There is a well-known relationship between the critical damping ratio of a mode in a viscously damped system and the frequencies of the zero real displacement mobility slopes. This relationship requires the assumption that the peak frequencies are negligibly affected by other modes.

Setting the derivative of the real acceleration mobility (Equation 12) with respect to frequency equal to zero, we find that Soroka structural damping coefficient is given for real acceleration mobility by the same equation that gives the viscous critical damping ratio for displacement mobility.

$$g_i \cong \frac{\dfrac{\omega_U{}^2}{\omega_L{}^2} - 1}{\dfrac{\omega_U{}^2}{\omega_L{}^2} + 1} \tag{42}$$

where U refers to the mobility minimum and L refers to the mobility maximum.

From Equation (11) we see that the Soroka structural damping coefficient can be approximated using the peak imaginary acceleration mobility, $\overset{..}{Y}{}^I_{jk\Omega}$ , occurring at resonance and the modal acceleration.

$$g_i = \frac{A_{jki}}{\overset{..}{Y}{}^I_{jk\Omega_i}} \tag{43}$$

## Comparison of Methods of Obtaining Modal Acceleration

Computer experiments using moderately high structural damping and physical experiments of a very lightly damped specimen in this contract show that the iterative methods (given reasonable start estimates) tend to converge with acceptable accuracy almost immediately. In both iterative methods, the calculations converge, not on a "true" value as in Stodola iteration, but on the minimum sum of the sequence of residuals needed to balance the equation. In both iterative methods, the accuracy of the answers is a function of the accuracy of the initial "first approximations". Particularly for low damping, the convergence aspects of the iterative methods do not appear to be of paramount importance, if the input data to either process is accurate.

The only criterion for acceptability of answers should not be minimization of the norm of the residuals unless there is no practical way of separating probably inaccurate test data from probably accurate test data. The minimization of the residual norms is a least squares fit and gross error in one datum input out of many data input can create large errors in all the answers. On the other hand, the iterative methods are very beneficial when the first approximations are reasonable and when there are no "outlying bad" input data.

30

A combination of deterministic methods using different input data (to indicate curiously inconsistent, and probably excessively erroneous, input data to be either rechecked or discarded) and the iterative methods which average the data is the preferred approach whenever possible.

The two deterministic methods discussed are the antiresonance theory equation and Equation (38) with a square S matrix. It is desirable to use both. The antiresonance equation provides a physical insight, allows conclusions to be drawn from inspection of the data and can be calculated by hand. However, it does not allow flexibility in choosing the data and is unsuitable for automated testing. Equation (38) with a square S matrix permits selection of different mobility levels, can then be expanded by degrees to increasingly larger levels of nondeterminism (i.e., more forcing frequencies than modes) and is convenient for automated testing. However, it provides no physical insight, reveals little from inspection of the data and, in general, cannot be calculated by hand.

The antiresonance equation can be used to check key curves in an approximate manner so that the engineer satisfies himself that the measured mobility is physically reasonable, while Equation (38) with square S matrix and various data points is used for the actual numerical filtering of outlying data using an on-line computer before using a pseudoinverse reduction.

Of the two iterative approaches discussed, pseudoinverse iteration, using either the real or imaginary mobility, depending on light or heavy damping, with all accelerometer readings (per unit force) at the same frequencies, is the method most convenient when there are many accelerometers and when the data taking is highly automated. The technique which uses the pseudoinverse of the real acceleration mobility and the solution of the damping coefficient from the imaginary mobility for each accelerometer independently (Reference 12) is preferable when it is possible to treat each accelerometer independently.

Test data can never be blindly accepted as accurate anymore than analytical predictions can be blindly accepted as realistic. The chances of errors in calibration, unrecorded disturbance in equipment settings, unexpected noise, transducer malfunction, human error in applying factor and other such things comprise a factorial chain of inherently low reliability of test data. The engineer should select such combinations of data reduction methods that allow him the maximum economy of data processing while giving him the

maximum capability of cross-checking the data. This checking
of data should, of course, be of a nature that depends on the
physics of the specimen, whenever possible, as opposed to
checks dependent on links in the processing chain. The
optimum economy of the total test project, in contrast to the
economy of the data processing alone, is enormously magnified
by physical checks on the data being done on-site and during
the testing as the setup costs, resetup costs and costs of
erroneous conclusins drawn from erroneous data greatly out-
weigh the costs of processing data or doing the testing.

## IDENTIFICATION OF FULL MOBILITY MATRIX FROM SINGLE-POINT SHAKING

The responses of a helicopter structure to many different
excitations are required to fully evaluate its dynamic
performance. It is obvious that we need the response of
the entire fuselage to each of the three forces and moments
at the main rotor hub and at the tail rotor hub (or at both
main rotors in a tandem) which customarily requires twelve
different shaker locations. If there is a dynamic absorber
in the fuselage, we need to know the driving point impedance
of the ship at the absorber attachment to determine the
required size of the abso ber and this presently means a
thirteenth shaking station. In addition, engineers have an
increasing need to know the impedance from forcing at such
other points as engine supports, transmission mounts, ex-
ternal stores attachments, etc., to fully utilize the power-
ful analytical tools of impedance methods. Because shaker
changeover time is a major cost of a shake test program, we
may regard each change of shaker position as a shake test in
itself. It is obviously impractical, from cost and schedule
considerations, to shake at every point on a helicopter at
which driving point impedances (or mobilities) are desired.

It is possible to obtain the impedance data relative to a
force at any point at which there is an accelerometer from
single-point forcing, and it is not necessary to obtain the
equations of motion to do this. Therefore, with only one*
shake test, the engineer can obtain all of the desired
impedance test data that presently requires dozens of tests.

---

* To assure that all the driving point modal accelerations
  are sufficiently large in the shake test of a complete
  fuselage, the engineer would use single-point shaking
  theory for a combination of several convenient shaking
  points.

Note that modal accelerations for any given mode satisfy reciprocity, $A_{jki} = A_{kji}$, and that, for excitation at e, any driving-point or transfer modal acceleration is given by:

$$A_{jki} = \frac{A_{jei} A_{kei}}{A_{eei}} \qquad (44)$$

If we had an accelerometer at j and at k, and the shaker at e, we could obtain the mobility at j for a force at k by using Equation (44). Then

$$\ddot{Y}_{jk\omega} = E_{jk} + \sum_{i=Z+1}^{N} A_{jki} \frac{(1 - \omega^2/\Omega_i^2) + ig_i}{(1 - \omega^2/\Omega_i^2)^2 + g_i^2} \qquad (45)$$

As will be shown later, the validity of this procedure was experimentally demonstrated as part of this contract.

## IDENTIFICATION OF STATIC TEST LOADS AND DEFLECTIONS

In the static strength testing of a helicopter, four types of loading are applied to the suspended fuselage to simulate the strains and deflections which would occur in a maneuver critical to the strength of the ship: airloads; engine, and transmission mount reactions; inertial loads of concentrated mass items (e.g., engines, transmission, t.r. gearbox, etc.); and inertial loads of the distributed structure. The last of these may comprise 50 percent of the stripped aircraft weight and are quite difficult to calculate; the engineer must lump the distributed inertial g-loading of intercostals, skin, stringers, flooring, and keels at relatively few points, perhaps five, along and about the fuselage. He most often does this solely by judgment.

Using test data from our tubular specimen, we will demonstrate below how the lumped g-loadings to be applied as forces in static strength testing can be determined rationally in the process of system identification.

During static strength testing of an aircraft, the deflections are measured generally by sighting deflection scales attached to the ship using a telescopic transit. These deflections through the linear range can be determined very accurately in the process of system identification and would then not only provide an independent check on the validity of the static strength test but give baseline deflections, departures

from which would indicate the beginnings of structural
yielding in the strength test.

For the given critical maneuver (e.g., 3-g rolling pullout),
the external trim forces (e.g., main rotor shears and
moments, tail rotor thrust, torque, etc.) are given. Post-
multiplying the free-body influence coefficient matrix by
these external forces yields the deflections of the aircraft
relative to inertial axes under the g-loadings of the man-
euver. These deflections may be geometrically transformed
to be relative to any statically determinate set of points
which may be considered of zero deflection (or rotation),
being the points relative to which the deflections in the
static strength test are measured. These deflections should
be the same as those measured in static strength tests below
the yield point of the structure.

$$[C_{FIC}]\{f_{external}\} = \{\delta\} \qquad (46)$$

The free-body influence coefficients determined in system
identification test are transformed to static influence
coefficients with constraints at the zero deflection base
points from which the test fuselage is suspended. The
concentrated forces to be applied in the static strength
test to most closely approximate the distributed inertial
g-loadings of the critical maneuver are given by:

$$[C_{SIC}]^{-1}\{\delta\} = \{f\} \qquad (47)$$

This technique has been experimentally demonstrated under
this contract, and the results are shown in another section
of this report.

## IDENTIFICATION OF STATIC INFLUENCE COEFFICIENTS FROM FREE-BODY TESTING

Free-body influence coefficients are not a purely elastic
property of a helicopter because they are a function of the
rigid-body inertial properties. Static influence coeffi-
cients, the classical measurable of static structural
analysis, are purely elastic properties, but static influence
coefficients are all infinite for a free body such as a
flying helicopter. In analysis of free structures, the
static influence coefficients of a structure, determinis-
tically constrained at arbitrary points, are often calculated
and then transformed to give free-body influence coefficients
so that the dynamics of the unrestrained structure can be

34

analyzed (Reference 1).

The reverse process of using free-body test data to obtain static influence coefficients of the structure with arbitrary restraint has long been of importance to all branches of the aerospace industry; Rodden (Reference 7) succeeded in doing this for a delta wing but he had to use an intuitive (i.e., unmeasured) mass matrix. In many helicopter structures, particularly in center fuselage sections with large doors, in irregular spacecraft like the Shuttle, and in any complicated structure in which to measure only a small number of degrees of freedom, we need to avoid the assumption of a lumped parameter mass matrix.

It was experimentally demonstrated under this contract that Static Influence Coefficients for arbitrary determinant restraints may be obtained from impedance test data on a free structure without assumptions of the mass matrix.

To do this, we construct a nonsingular matrix, consisting only of geometric terms, relating the coordinates of restraint to rotations about and displacements along an arbitrary coordinate system. This matrix, which we call $S_R$, cannot be of order greater than six, say $Z$. We also construct a purely geometric matrix, which we call $S_A$, such that the forces of restraint, indicated by the subscript R, are related to forces which could be applied to the free coordinates, indicated by the subscript, F, by

$$\{f_R\} = [S_R]^{-T}[S_A]^T\{f\} \tag{48}$$

Having obtained the free-body influence coefficients for both the restrained coordinates, subscript R, and the free coordinates, subscript F, we may calculate the static influence coefficient matrix from

$$[C] = [C_{FF}^E + S_A S_R^{-1} C_{RR} S_R^{-T} S_A^T - C_{FR}^E S_R^{-T} S_A^T - S_A S_R^{-1} C_{RF}^E] \tag{49}$$

35

## IDENTIFICATION OF INERTIAL AND ELASTIC PROPERTIES

A term in the inverse of the mass matrix (Reference previous contract) is defined as the inertial coefficient and is given by

$$I_{jk} = \sum_{i=1}^{N} A_{jki} = E_{jk} + \sum_{i=Z+1}^{N} A_{jki} \tag{50}$$

We can use antiresonance theory directly on the plots to check each inertial coefficient which has the shaking station, e, as one of the subscripts.

$$I_{je} = (E_{je} + K) \frac{\prod_{i=Z+1}^{N} \Omega_i^2}{\prod_{i=Z+1}^{N} a_{jei}} - K \tag{51}$$

In forming the mass matrix the number of modes, N, should be no greater than the number of stations, J. The mass matrix is then given by

$$[m] = [A]^{+T} [A_{eei}] [A]^{+} \tag{52}$$

where the matrix A has J rows and N columns. For the same number of stations as modes, J=N, the mass matrix is the inverse of the Inertial Coefficient matrix.

$$[m] = [I]^{-1} \tag{53}$$

Similarly, the stiffness matrix is given by

$$[k] = [A]^{+T} [A_{eei}\Omega_i^2] [A]^{+} \tag{54}$$

and in this case, as opposed to the case of the mass matrix, the A matrix must include the rigid-body modes. The rigid-body modal accelerations are obtained in the manner in which the rigid-body acceleration coefficient, which is simply a sum of the rigid-body accelerations coefficients. is calculated. Partitioning the diagonal matrix of Equation (54) into rigid-body and nonrigid-body parts, we may rewrite Equation (54) as Equation (55).

$$[k] = [A]^{+T} \begin{bmatrix} 0 \\ \hline & A_{eei}\Omega_i{}^2 \end{bmatrix} [A]^+ \qquad (55)$$

When the number of stations J is greater than the number of modes N, we have a "truncated model" which is a form of "incomplete model" (Reference 14). In general, the engineer will be using many more stations than modes and will be using truncated models. The method of calculating the effects of changes in truncated models is shown in the appendix.

# TEST EQUIPMENT AND SPECIMEN

## SYSTEM IDENTIFICATION TEST EQUIPMENT

The data acquisition and recording system used in the test program consisted of the following equipment: Wilcoxon Model Z602 Impedance Head, Endevco Model 2272 and 2232C Accelerometers, Kistler Model 504A Electrostatic Charge Amplifiers, Spectral Dynamics Model SD1002E Automatic Mechanical Impedance Analysis System, and a Hewlett Packard Model 136A Recorder. The force excitation system consisted of a Ling Electronics Model 411 Electromagnetic Exciter powered by an MB Power Amplifier.

The Automatic Mechanical Impedance Analysis System included the following units: SD109B CO/Quad Analyzer, SD 112-1-H Voltmeter/Frequency Log Converter, SD 122 Two-Channel Tracking Filter Slave, SD 127 Mechanical Impedance-Transfer Function Analysis Control, SD 104A-5 Linear/Log Sweep Oscillator, SD 105B Amplitude Servo/Monitor, SD 121S Tracking Filter Slave.

The SD 1002E is a complete self-contained system using one oscillator reference, accepts two signal inputs for complete operation, and yields the quadrature and in-phase components of the dynamic response. Figure 6 presents a schematic diagram of the test configuration.

The impedance head, capable of measuring the force excitation and resulting acceleration at a common point, was attached to the test specimen with a NO 10-32 stud with two brass washers placed between the impedance head surface and the test specimen. The impedance head used has a small specimen contact area, thereby minimizing local stiffening of the specimen at the attachment point. The impedance head is also characterized by low mass below the force gage minimizing the dynamic mass contribution of the impedance head. To further reduce the constraining effects of the impedance head, the exciter was coupled to the impedance head by a flexible mechanical fuse allowing the specimen freedom of motion.

The accelerometers used in the investigation were self-generating piezoelectric type requiring no external power for operation. The transducers were attached to the test specimen by means of a NO 10-32 mounting stud with two brass washers inserted between the accelerometers and the test specimen.
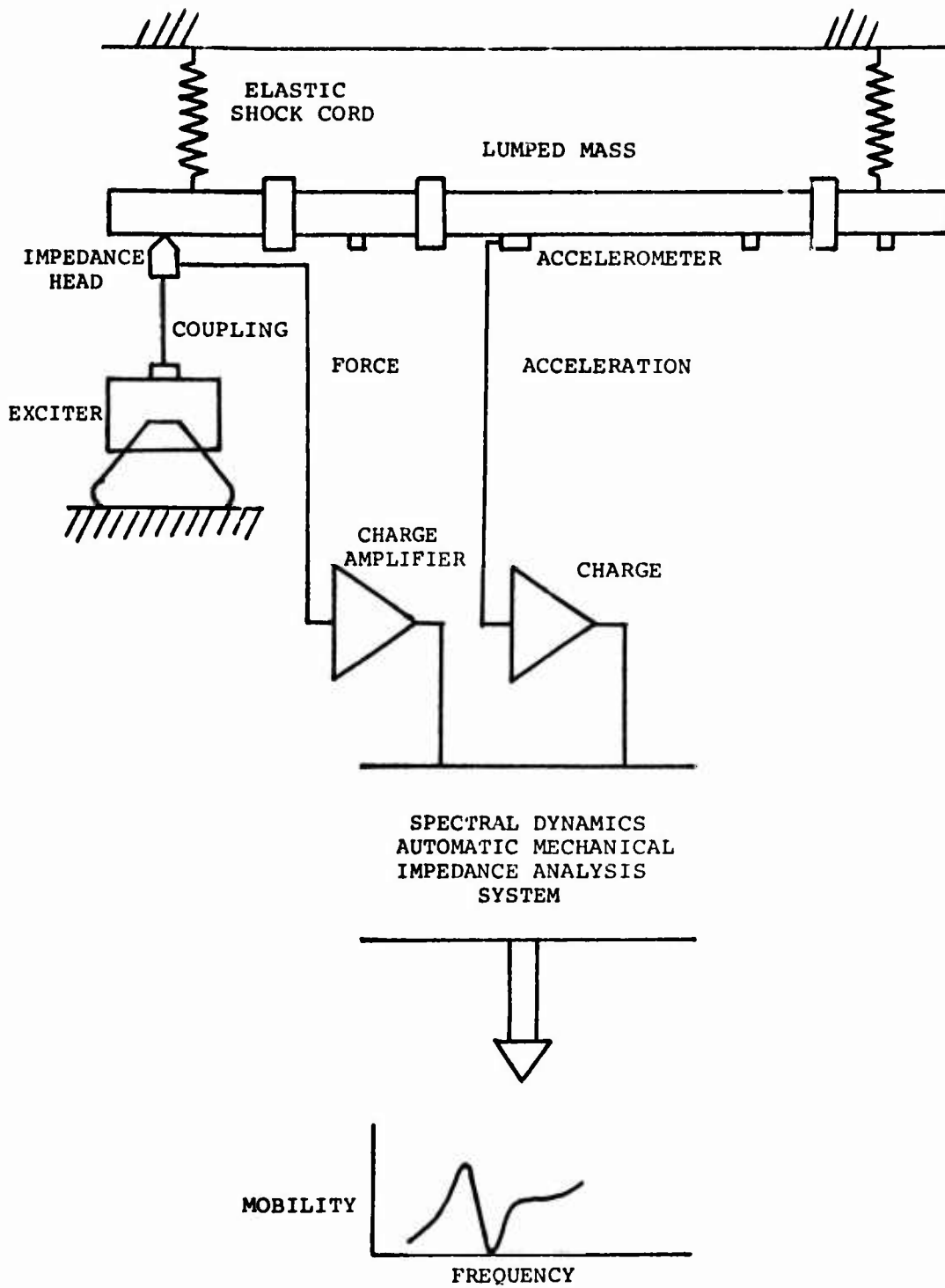
38

Figure 6.    Schematic of Test Configuration.

39

The transducer output response was directed to the electrostatic charge amplifiers for signal conditioning. Since there were only two charge amplifiers available for the test program, one charge amplifier was reserved for the response from the force gage while the signals from the accelerometers measuring the driving point or transfer point responses were manually switched into the remaining charge amplifier as required.

The conditioned force and acceleration signals were input to the Spectral Dynamics Automatic Mechanical Impedance System. The system reduced the dynamic test data yielding the vector components of the acceleration mobility response, the quadrature, and the in-phase data necessary to the system identification analysis. The output signals from the Mechanical Impedance Analysis System were channeled to the Hewlett Packard Analog Recorder yielding effectively real time observation of the dynamic response of the test specimen. Figure 7 presents a photograph of the test setup. The impedance and a typical acceleration transducer are shown in Figure 8.

SPECIMEN

An analytical parametric study, using an IBM Model 360/40 Computer, was conducted to determine the physical characteristics of a beam test specimen suitable for structural system identification. Using a lumped mass representation of a continuous beam and using classical theory for vibration of a slender beam in bending the physical parameters, constraint condition, frequency spectrum for the modes of interest, and dynamic response were determined for a practical test specimen design.

The specimen chosen for the test program was a 75-inch steel beam of hollow circular cross-section with cylindrical shaped lumped masses attached at three span locations. The system was suspended by low spring rate elastic cord (bungee) to assure that the highest rigid-body natural frequency was significantly below the first elastic natural frequency of the test beam, thus simulating the free-free boundary conditions of a helicopter flight. The test specimen was originally suspended by coil springs of very low spring rate; however, during test runs spring resonances were encountered which affected the dynamic response of the specimen. These spring resonances appeared throughout the frequency spectrum; therefore, to avoid the situation the test beam was suspended by low spring rate shock cord. Figure 9 presents a description of the test specimen.
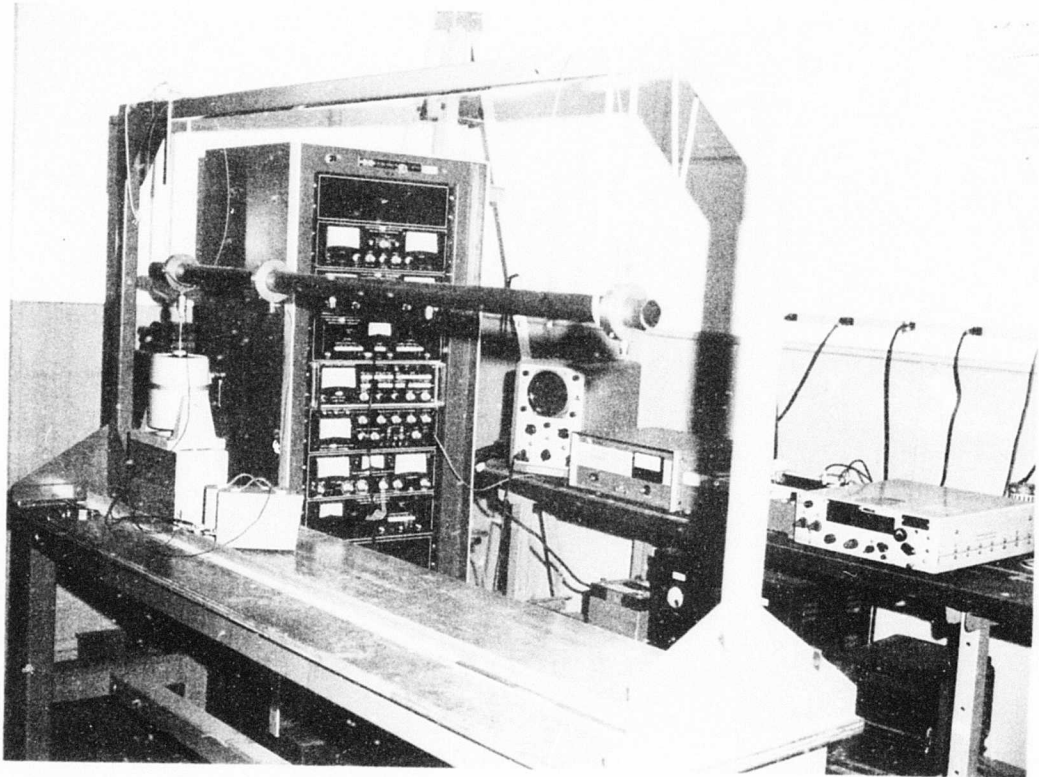
Figure 7.    Test Setup.
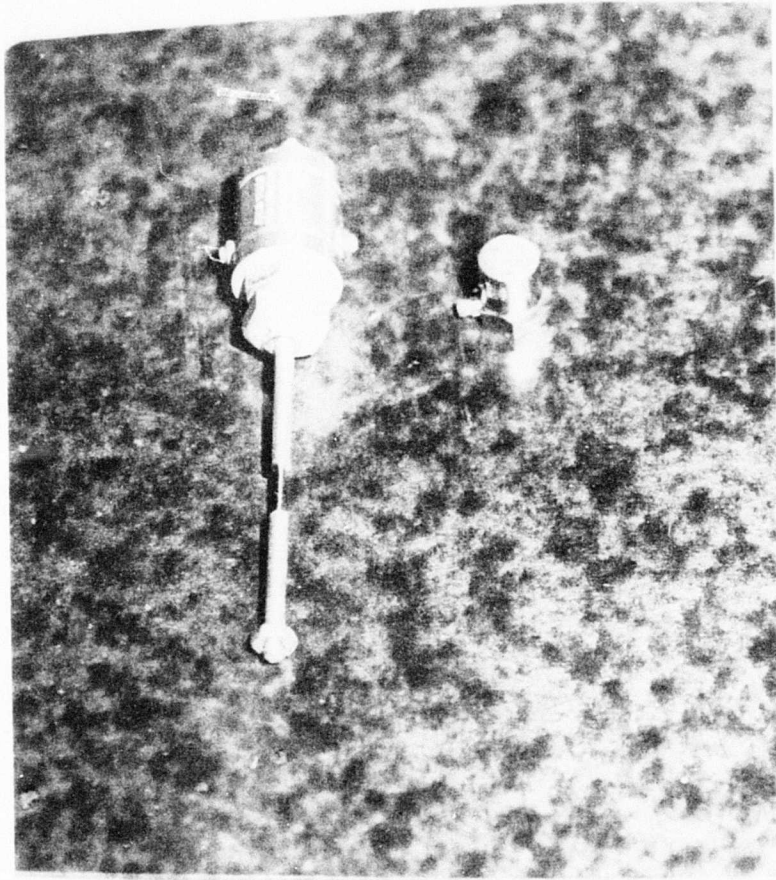
Figure 8.   Impedance Head and Typical Accelerometer.

42

ENLARGED VIEW
A-A

WALL THICKNESS
± .0125
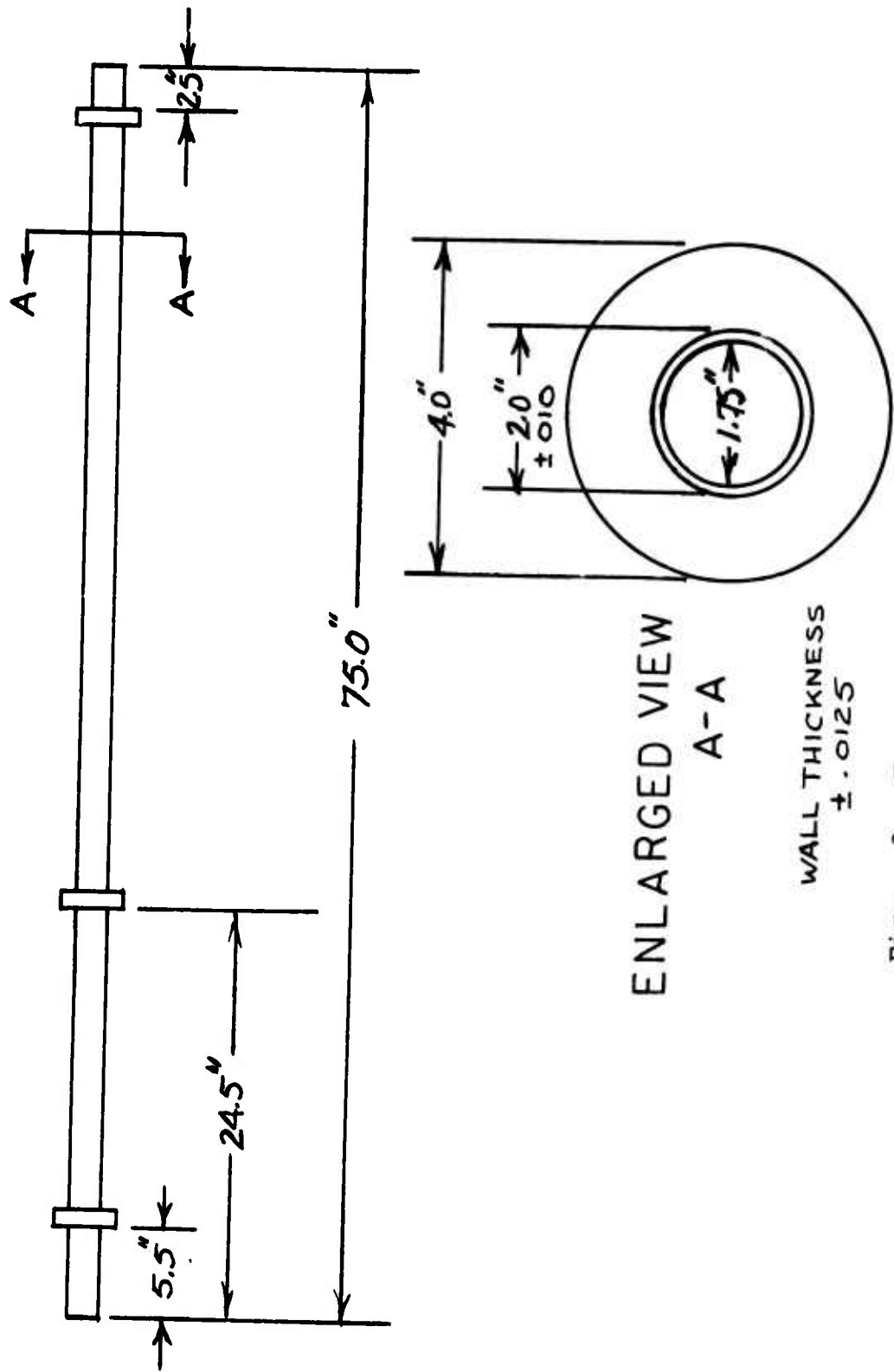
Figure 9. Test Specimen.

43

A fundamental model of the type used in the test program minimizes the extraneous effects of force excitation misalignment and boundary condition, while allowing the excitation frequency to remain within a reasonable level sufficient to achieve dynamic response over the modal range of interest.

The model was also amenable to analytical identification using classical theory for vibration of a beam in bending. This facilitated a comparison between the dynamic response calculated for the model extracted from actual test results using system identification techniques and the dynamic response obtained for the model using analytical methods.

## TEST PROCEDURES

### TEST PROCEDURE

The test procedure required the selection of points of interest on the model which would yield the greatest dynamic response for a given force input level. These points were selected on the basis of analytical calculations. Motion transducers were placed at each selected point and oriented so that the action of the impressed force was coincident with the principal direction of the transducer at the point of interest. Force excitation was applied over a frequency spectrum encompassing the modes of interest, being equal to or less than the number of points of interest. In recording the dynamic response of the points of interest, the total frequency spectrum was divided into several bandwidths, each surrounding one of the natural frequencies of the system. This procedure allowed greater definition of the dynamic response in the region of a natural frequency.

One further consideration which affects the recording of the dynamic response of the test specimen is the frequency sweep rate. The frequency must be swept at a rate to assure full excitation of resonant conditions. The sweep rate was set at the lowest possible rate consistent with the aforementioned requirement; however, the sweep rate must be maintained at a high enough level to provide good character of line from the analog recorder. An oscilloscope was used to continuously monitor the dynamic response and force signals to assure that instrumentation saturation was not occurring and that the signals were of sufficient level to yield adequate output parameter resolution.

For each frequency bandwidth the individual accelerometer transducer outputs were selectively directed to the charge amplifier, and the mobility response of each point was recorded. The same procedure was used for each successive frequency bandwidth until the complete frequency spectrum was traversed.

## CALIBRATION PROCEDURE

The technique used for system calibration involved observation of the system response for a known input condition. A transducer was mounted on a static mass of known value and the combination was mounted on the impedance head coupled to the exciter. With the charge amplifiers set at appropriate amplification levels and the analog recorder set at a prescribed sensitivity level (millivolts/inch), the known mass was excited over the frequency range of interest. The system mobility response obtained from the automatic mechanical impedance analysis system was recorded on the analog recorder yielding a calibration line for the particular transducer. This procedure was followed for each of the transducers, thus, a calibration line was established for each transducer. Physical significance could be applied to the actual test results of the specimen by relating to the calibration line associated with each transducer.

# TEST RESULTS

## SELECTION OF DATA POINTS

By inspection of Equations (24) and (31) we see that real acceleration mobility values which are close to the value of the rigid-body acceleration coefficient, E, will involve use of what is commonly called "small differences of large numbers" and will magnify the effect of measurement errors (noise) in the calculation of the modal accelerations. This effect is very important in testing because practical engineering measurements of acceleration, and therefore mobility, are at best accurate to something less than two significant figures.

To maximize the accuracy of the calculation, we choose values of mobility which are not close to the value of the rigid-body acceleration coefficient. An obvious, but not necessary, choice would be to use acceleration mobility values which are opposite in sign to the RAC. In this testing, we used both positive and negative values of mobility, being certain that the mobility was never nearly equal in magnitude to the RAC. However, we generally chose mobility values which were opposite in sign from the RAC, whenever other constraints allowed, because it simplified the choice of data points.

Frequencies can be determined more accurately than mobilities. Using a servo oscillator, one can dwell at a frequency and use an electronic counter to read out the frequency to as many digits as the counter is capable of displaying within the ordinarily very narrow limits of hunting of the servo control. We did not use the electronic counter for this purpose, however, because the time which would be required to obtain the precision possible with a counter was impractically long. We used the counter to calibrate the frequency scale on the automatic plotter and read frequency from the mobility graphs.

Frequency presents another condition for the minimization of measurement errors, or noise, in data reduction. In Equation (30) we see that mobility measured at a forcing frequency very near the natural frequency gives a ratio very nearly one which must be subtracted from one in forming the S matrix and could, therefore, lead to large errors. To maximize the accuracy of the data reduction, we therefore chose forcing frequencies as far as possible from the natural frequencies.

Whenever there was an antiresonance, the antiresonant frequency was used because this eliminated the effect of errors of the calibration factor on the associated mobility. Antiresonant frequencies are the exception to the rule that mobility data should be taken at frequencies as far away as possible from natural frequencies. As shown by Equation (23), when there is an antiresonance very near a natural frequency, it is a physical fact that the modal acceleration of that mode, for the given accelerometer and shaking station, is small; i.e., it is what is called a "minor" mode for the stations in question.

Obviously, the data points must be distributed throughout the spectrum under consideration to insure that the modes are nearly equally well weighted.

## NATURAL FREQUENCIES

The natural frequencies of an idealized 20-degree-of freedom Bernoulli-Euler model of the free specimen were calculated by formulating the free-body influence coefficients and iterating to obtain the lowest nonzero natural frequency first. The first time, calculated natural frequencies compared reasonably well with the five measured natural frequencies.

|  | Natural Frequencies (Hz) | | | | |
|---|---|---|---|---|---|
| Mode: | I | II | III | IV | V |
| Calculated by Bernoulli-Euler Beam Theory 20 Pt Model | 65.113 | 189.819 | 436.332 | 714.302 | 1062.649 |
| Measured from Mobility Plots | 65.5 | 186.0 | 413.0 | 662.0 | 937.0 |

As one would expect, the theoretical predictions of natural frequencies are most accurate for the lowest modes.

## MODAL ACCELERATIONS AND DAMPING

Modal accelerations for each of five modes were obtained for five stations with the shaker at station 72.5 inches and for six stations with the shaker at station 0.5 inch in two ways:

(1)  With various combinations of five forcing frequencies dispersed through the five mode spectrum using antiresonance theory and Equation (37).

(2)  Using the pseudoinverse method of Equations (37) through (41). Because the damping in the specimen is extremely light, the modal accelerations changed little with iteration, and there was no apparent advantage to iterating to obtain modal accelerations.

Damping values were calculated by iteration of Equations (37) through (41) and it was found that the values of damping generally became divergent, instead of convergent, after about six iterations. In nearly every case, the iterative process was halted by the $SS^T$ matrix becoming singular. The damping of the specimen is so low that the procedure might be considered largely an operation in the noise "grass". The first approximations to the values of structural damping coefficient seemed to be reliable, judging from effects on modal accelerations in the low ordered iterations and the stability of the calculations, and in only 9 cases out of 55 did the damping coefficient get above 1 percent with a maximum of 1.61 percent. The average structural damping coefficient obtained in shaking at the 72.5-inch station was 1/4 percent and in shaking at the 0.5-inch station it was 0.7 percent.

Computer experiments (Reference 5) with 5 percent damping and higher showed that iteration was not essential to accuracy. The results of physical experiments of this contract support that conclusion with the further indication that iteration may be detrimental, at least in cases of low damping, to results of iteration calculations not proven to be necessarily convergent (Reference 12).

The modal accelerations for force at 72.5 inches obtained with the shaker at the 72.5-inch station, shown in Table 1, compare quite well with the modal accelerations for force at 72.5 inches obtained with the shaker at the 0.5-inch station, nearly the other end of the specimen, shown in Table 2. Table 3 shows the modal accelerations for force at 72.5 inches, as calculated by Bernoulli-Euler beam theory for the specimen.

49

| TABLE 1. | MODAL ACCELERATIONS RELATIVE TO FORCING AT THE 72.5-INCH STATION IDENTIFIED FROM TEST DATA OBTAINED BY SHAKING AT THE 72.5-INCH STATION |
|---|---|

| In./Sec$^2$ Mode | | | | | |
|---|---|---|---|---|---|
| Station | I | II | III | IV | V |
| 6 in. | 23.16 | -9.40 | 2.09 | .94 | -1.67 |
| 25 in. | -18.56 | 17.86 | -3.49 | -3.50 | 5.96 |
| 35.5 in. | -33.32 | -.70 | 16.30 | -1.83 | -11.64 |
| 61 in. | -1.35 | -18.52 | -15.88 | -7.55 | -7.24 |
| 72.5 in. | 21.84 | 11.88 | 6.21 | 2.37 | 3.07 |

| TABLE 2. | MODAL ACCELERATIONS RELATIVE TO FORCING AT THE 72.5-INCH STATION IDENTIFIED FROM TEST DATA OBTAINED BY SHAKING AT THE 0.5-INCH STATION |
|---|---|

| In./Sec$^2$ Mode | | | | | |
|---|---|---|---|---|---|
| Station | I | II | III | IV | V |
| 6 in. | 26.08 | -8.74 | 1.84 | .79 | -1.80 |
| 25 in. | -19.16 | 17.42 | -4.30 | -4.84 | 4.65 |
| 35.5 in. | -32.46 | .71 | 20.00 | -1.93 | -9.61 |
| 61 in. | -2.48 | -17.11 | -20.26 | -7.45 | -5.28 |
| 72.5 in. | 28.18 | 12.64 | 7.38 | 2.05 | 1.82 |

| TABLE 3. | MODAL ACCELERATIONS RELATIVE TO FORCING AT THE 72.5-INCH STATION CALCULATED BY BERNOULLI-EULER BEAM THEORY FOR THE SPECIMEN |
|---|---|

| In./Sec$^2$ Mode | | | | | |
|---|---|---|---|---|---|
| Station | I | II | III | IV | V |
| 6 in. | 21.34 | -8.02 | 1.81 | .89 | -2.20 |
| 25 in. | -16.49 | 16.47 | -3.18 | -5.25 | 4.80 |
| 35.5 in. | -25.44 | .52 | 17.98 | -2.28 | -11.64 |
| 61 in. | -1.75 | -16.72 | -18.36 | -8.55 | -7.19 |
| 72.5 in. | 21.89 | 11.89 | 6.4- | 2.46 | 2.34 |

Comparing Table 4 to Table 5, we see that the identified
modal accelerations relative to a force at station 0.5 inch,
obtained by shaking at station 0.5 inch, are essentially those
obtained for this specimen by Bernoulli-Euler beam theory.

TABLE 4. MODAL ACCELERATIONS RELATIVE TO FORCING AT THE
0.5-INCH STATION IDENTIFIED FROM TEST DATA
OBTAINED BY SHAKING AT THE 0.5-INCH STATION

| Station | In./Sec$^2$ Mode | | | | |
|---|---|---|---|---|---|
| | I | II | III | IV | V |
| 0.5 in. | 52.12 | 38.16 | 49.32 | 122.89 | 86.08 |
| 6 in. | 35.47 | 15.18 | 4.75 | -6.144 | -12.36 |
| 25 in. | -26.06 | -30.27 | -11.10 | 37.50 | 32.04 |
| 35.5 in. | -44.14 | -1.23 | 51.67 | 14.92 | -66.15 |
| 61 in. | -3.37 | 29.72 | -52.36 | 57.68 | -39.32 |
| 72.5 in. | 38.33 | -21.97 | 19.08 | -15.87 | 12.51 |

TABLE 5. MODAL ACCELERATIONS RELATIVE TO FORCING AT THE
0.5-INCH STATION CALCULATED BY BERNOULLI-EULER
BEAM THEORY FOR THE SPECIMEN

| Station | In./Sec$^2$ Mode | | | | |
|---|---|---|---|---|---|
| | I | II | III | IV | V |
| 0.5 in. | 53.31 | 40.11 | 50.67 | 134.70 | 88.23 |
| 6 in. | 33.30 | 14.73 | 5.09 | -6.59 | -13.53 |
| 25 in. | -25.73 | -30.24 | -8.96 | 38 86 | 29.49 |
| 35.5 in. | -39.70 | -.10 | 50.60 | 16.88 | -71.52 |
| 61 in. | -2.73 | 30.71 | -51.68 | 63.27 | -44.18 |
| 72.5 in. | 34.16 | -21.84 | 18.00 | -18.19 | 14.36 |

The columns of the modal accelerations, as shown in the
tables, are the classical normal modes (i.e., elements in
the eigenvectors of $k^{-1}m$) and the reciprocal of the modal
accelerations at the driving point are the generalized
masses.

## IDENTIFIED INERTIAL AND ELASTIC PROPERTIES OF THE FREE SPECIMEN

In identifying the free-body inertial and elastic properties from the test data obtained in this contract, we concentrated on the matrices with the rigid body modes eliminated. Because the rigid-body modal parameters are known before testing aircraft fuselages and major components, and were calculated independently of the testing in these experiments, inclusion of the rigid-body modes in these identifications, where possible, would exaggerate the accuracy of the actual identifications from test data alone. There is also some numerical economy in working with these matrices of elastic modes and incorporating the known rigid body modes in constructing the mobilities although the advantage is not very significant.

The product of the free-body influence coefficient matrix and the inertial coefficient matrix of the nonzero modes (which is the inverse of the mass matrix limited to elastic modes) has eigenvalues which are the nonzero natural frequencies. The natural frequencies calculated by iteration on this matrix are not shown because they are exactly the same as the measured natural frequencies.

Identifications were made for two five-degree-of-freedom models with five modes: (1) from data obtained with the shaker at the 72.5-inch station, and (2) from data obtained with the shaker at the 0.5-inch station. The five-degree-of-freedom model consisted of stations at 6, 25, 35.5, 61 and 72.5 inches. Identifications were also made for a model of six-degrees-of-freedom having only five modes from test data with the shaker at station 0.5 inch.

## IDENTIFIED INERTIAL COEFFICIENT MATRIX OF THE 5X5 MODEL

From the 20 x 20 Bernoulli-Euler intuitive model of the specimen, we calculated the following matrix of elastic inertial coefficients of the five-degree-of-freedom model for five modes.

$$\begin{bmatrix} 72.46 & & & \text{Symmetric} & \\ -7.80 & 78.30 & & & \\ 7.55 & 8.91 & 156.79 & & \\ 3.19 & -.67 & 9.38 & 162.09 & \\ -1.11 & 1.11 & -5.22 & -10.50 & 98.97 \end{bmatrix} \quad \frac{\text{in.}}{\text{lb-sec}^2}$$

From test data taken with the shaker at the 72.5-inch station, the following elastic inertial coefficient matrix was identified for the five-degree-of-freedom model for five modes.

$$
\begin{bmatrix}
77.32 & & & & \\
-12.92 & 81.77 & & \text{Symmetric} & \\
-6.20 & 15.14 & 155.87 & & \\
3.98 & -12.13 & 10.76 & 144.69 & \\
.183 & 3.03 & -15.54 & -8.47 & 99.36
\end{bmatrix}
\frac{\text{in.}}{\text{lb-sec}^2}
$$

From test data taken with the shaker at the 0.5-inch station, the following elastic inertial coefficient matrix was identified for the five-degree-of-freedom model for five modes.

$$
\begin{bmatrix}
76.61 & & & & \\
-10.86 & 84.46 & & \text{Symmetric} & \\
.52 & 7.33 & 160.88 & & \\
2.41 & 2.09 & -2.08 & 155.71 & \\
3.40 & -1.34 & -7.65 & -10.65 & 106.09
\end{bmatrix}
\frac{\text{in.}}{\text{lb-sec}^2}
$$

## IDENTIFIED MASS MATRIX FOR THE 5X5 MODEL

From the 20 x 20 Bernoulli-Euler intuitive model of the specimen, we determined the following mass matrix for five elastic modes of the 5x5 model.

$$
\begin{bmatrix}
.772 & & & & \\
.402 & .229 & & \text{Symmetric} & \\
.004 & .005 & .009 & & \\
-.197 & -.097 & .004 & .068 & \\
-.433 & -.217 & .007 & .134 & .298
\end{bmatrix}
\frac{\text{lb-sec}^2}{\text{in.}}
$$

From test data taken with the shaker at the 72.5-inch station, the following mass matrix, for the elastic modes, was identified for the five-degree-of-freedom model for five modes.

$$
\begin{bmatrix}
1.015 & & & & \\
.580 & .352 & & \text{Symmetric} & \\
.065 & .042 & .017 & & \\
-.190 & -.096 & -.001 & .067 & \\
-.483 & -.258 & -.010 & .134 & .315
\end{bmatrix}
\frac{\text{lb-sec}^2}{\text{in.}}
$$

From test data taken with the shaker at the 0.5-inch station, the following mass matrix, for the elastic modes, was identified for the five-degree-of-freedom model for five modes.

$$
\begin{bmatrix}
.629 & & & & \text{Symmetric} \\
.322 & .183 & & & \\
.019 & .013 & .010 & & \\
-.166 & -.080 & .001 & .063 & \\
-.342 & -.167 & 0 & .114 & .236
\end{bmatrix}
\quad \frac{\text{lb-sec}^2}{\text{in.}}
$$

## IDENTIFIED FREE-BODY INFLUENCE COEFFICIENT OF THE 5X5 MODEL

From the Bernoulli-Euler model of the specimen, the following free-body influence coefficients were calculated for the 5x5 model for five modes.

$$
\begin{bmatrix}
1.28 & & & & \text{Symmetric} \\
-1.04 & .912 & & & \\
-1.48 & 1.14 & 1.85 & & \\
-.03 & -.07 & .06 & .26 & \\
1.22 & -.88 & -1.50 & -.25 & 1.40
\end{bmatrix}
\quad \frac{\text{in.}}{\text{lb}} \times 10^4
$$

From test data taken with the shaker at the 72.5-inch station, the following free-body influence coefficients were identified for the 5x5 model for five modes.

$$
\begin{bmatrix}
1.51 & & & & \text{Symmetric} \\
-1.27 & 1.14 & & & \\
-2.07 & 1.65 & 3.08 & & \\
.01 & -.12 & .08 & .30 & \\
1.30 & -.97 & -1.95 & -.25 & 1.39
\end{bmatrix}
\quad \frac{\text{in.}}{\text{lb}} \times 10^4
$$

From test data taken with the shaker at the 0.5-inch station, the following free-body influence coefficients were identified for the 5x5 model for five modes.

$$
\begin{bmatrix}
1.50 & & & & \text{Symmetric} \\
-1.15 & .96 & & & \\
-1.79 & 1.29 & 2.30 & & \\
-.06 & -.05 & .09 & .29 & \\
1.50 & -1.01 & -1.89 & -.31 & 1.77
\end{bmatrix}
\quad \frac{\text{in.}}{\text{lb}} \times 10^4
$$

The free-body influence coefficients are heavily dominated by the lower modes.

## IDENTIFIED STIFFNESS MATRIX FOR THE 5X5 MODEL

From the Bernoulli-Euler model of the specimen, the following
matrix of stiffnesses, for the elastic modes, was calculated
for the 5x5 model for five modes.

$$
\begin{bmatrix}
13.48 & & & & \\
8.25 & 5.13 & & & \text{Symmetric} \\
-.59 & -.34 & .23 & & \\
-3.86 & -2.27 & .39 & 1.47 & \\
-7.92 & -4.76 & .62 & 2.63 & 5.07
\end{bmatrix}
\quad \frac{\text{lb}}{\text{in.}} \times 10^{-6}
$$

From test data taken with the shaker at station 72.5 inches,
the following matrix of stiffnesses, for the elastic modes,
was identified for the 5x5 model for five modes.

$$
\begin{bmatrix}
16.92 & & & & \\
10.75 & 6.93 & & \text{Symmetric} & \\
.379 & .294 & .235 & & \\
-3.55 & -2.089 & .222 & 1.297 & \\
-8.45 & -5.194 & .220 & 2.410 & 5.031
\end{bmatrix}
\quad \frac{\text{lb}}{\text{in.}} \times 10^{-6}
$$

From test data taken with the shaker at station 0.5 inch,
the following matrix of stiffnesses, for the elastic modes,
was identified for the 5x5 model for five modes.

$$
\begin{bmatrix}
9.24 & & & & \\
5.64 & 3.51 & & \text{Symmetric} & \\
-.152 & -.70 & .193 & & \\
-2.74 & -1.59 & .261 & 1.158 & \\
-5.22 & -3.11 & .340 & 1.89 & 3.33
\end{bmatrix}
\quad \frac{\text{lb}}{\text{in.}} \times 10^{-6}
$$

The stiffness matrices are dominated by the upper modes,
and comparisons of corresponding elements show significant
variation. However, these variations are not physically
significant as will be shown in the plots of the mobilities
resulting from the identified models.

## IDENTIFIED FREE-BODY INFLUENCE COEFFICIENTS OF THE 6X6 MODEL

Using the 20 x 20 Bernoulli-Euler intuitive beam model of
the specimen, we calculated the following 6x6 free-body
influence coefficient matrix for five modes.  This matrix
has, of course, a 5x5 submatrix of the FIC's of the five-
degree-of-freedom model.

$$
\begin{bmatrix}
3.62 & & & & \text{Symmetric} & \\
2.09 & 1.28 & & & & \\
-1.74 & -1.04 & .91 & & & \\
-2.31 & -1.47 & 1.13 & 1.85 & & \\
0 & -.03 & -.07 & .06 & .26 & \\
1.91 & 1.22 & -.88 & -1.50 & -.25 & 1.40
\end{bmatrix}
\quad \frac{\text{in.}}{\text{lb}} \times 10^4
$$

From the test data taken with the shaker at the 0.5-inch
station, the following free-body influence coefficients were
identified for five modes.

$$
\begin{bmatrix}
3.53 & & & & \text{Symmetric} & \\
2.23 & 1.50 & & & & \\
-1.75 & -1.15 & .96 & & & \\
-2.55 & -1.79 & 1.29 & 2.30 & & \\
-.04 & -.06 & -.05 & .09 & .29 & \\
2.12 & 1.50 & -1.01 & -1.89 & -.31 & 1.77
\end{bmatrix}
\quad \frac{\text{in.}}{\text{lb}} \times 10^4
$$

## IDENTIFIED STIFFNESS MATRIX FOR THE 6X6 MODEL

Using the 20 x 20 Bernoulli-Euler intuitive beam model of
the specimen, we calculated the following 6x6 stiffness
matrix using only five elastic modes.

$$
\begin{bmatrix}
5.88 & & & & \text{Symmetric} & \\
-5.75 & 11.29 & & & & \\
4.04 & 1.31 & 14.71 & & & \\
-4.30 & 14.56 & 5.84 & 23.05 & & \\
-4.36 & 15.35 & 13.50 & 21.90 & 32.45 & \\
-5.87 & 17.36 & 11.35 & 25.41 & 30.20 & 33.15
\end{bmatrix}
\quad \frac{\text{lb}}{\text{in.}} \times 10^{-4}
$$

56

From test data obtained with the shaker at the 0.5-inch station, we identified the following 6x6 stiffness matrix using only five elastic modes.

$$
\begin{bmatrix}
5.30 & & & & & \\
-4.68 & 8.89 & & \text{Symmetric} & & \\
3.42 & 1.22 & 12.11 & & & \\
-3.67 & 12.45 & 5.53 & 21.22 & & \\
-3.99 & 13.64 & 11.85 & 21.31 & 31.01 & \\
-5.07 & 14.63 & 9.84 & 23.39 & 28.12 & 29.68
\end{bmatrix}
\frac{\text{lb}}{\text{in.}} \times 10^{-4}
$$

## IDENTIFIED INERTIAL COEFFICIENTS FOR THE 6X6 MODEL

From the 20 x 20 intuitive Bernoulli-Euler beam model of the specimen, we calculated the following 6x6 inertial coefficient matrix for only five elastic modes.

$$
\begin{bmatrix}
420.88 & & & & & \\
81.17 & 72.46 & & \text{Symmetric} & & \\
31.94 & -7.81 & 78.31 & & & \\
-26.19 & 7.89 & 8.22 & 156.86 & & \\
-13.35 & 3.21 & -.66 & 10.06 & 162.16 & \\
5.87 & -1.11 & 1.10 & -5.69 & -10.49 & 98.86
\end{bmatrix}
\frac{\text{in.}}{\text{lb-sec}^2}
$$

From test data obtained with the shaker at the 0.5-inch station, the following 6x6 inertial coefficient matrix was identified for only five elastic modes.

$$
\begin{bmatrix}
402.47 & & & & & \\
86.42 & 76.61 & & \text{Symmetric} & & \\
31.99 & -10.86 & 84.46 & & & \\
-27.25 & .52 & 7.33 & 160.88 & & \\
-13.11 & 2.41 & 2.09 & -2.08 & 155.71 & \\
11.42 & 3.40 & -1.34 & -7.65 & -10.65 & 106.09
\end{bmatrix}
\frac{\text{in.}}{\text{lb-sec}^2}
$$

## IDENTIFIED MASS MATRIX FOR THE 6X6 MODEL

From the 20 x 20 Bernoulli-Euler model of the specimen, we calculated the following 6x6 mass matrix using only five elastic modes.

57

$$
\begin{bmatrix}
3.10 & & & & \text{Symmetric} & \\
-1.28 & 8.11 & & & & \\
-.98 & 1.61 & 18.57 & & & \\
.25 & 2.82 & 4.19 & 9.07 & & \\
-1.32 & 6.90 & 9.58 & 3.89 & 14.93 & \\
-3.37 & 14.81 & 18.49 & 8.14 & 17.10 & 41.51
\end{bmatrix}
\frac{\text{lb-sec}^2}{\text{in.}} \times 10^3
$$

From test data taken with the shaker at the 0.5-inch station, the following 6x6 mass matrix was identified using only five elastic modes.

$$
\begin{bmatrix}
3.34 & & & & \text{Symmetric} & \\
-1.30 & 6.87 & & & & \\
-1.07 & 1.27 & 17.00 & & & \\
0 & 3.31 & 4.86 & 10.00 & & \\
-1.53 & 6.90 & 9.58 & 5.88 & 16.41 & \\
-3.66 & 12.83 & 17.13 & 9.95 & 17.50 & 38.34
\end{bmatrix}
\frac{\text{lb-sec}^2}{\text{in.}} \times 10^3
$$

## EXPERIMENTAL DEMONSTRATION OF STATIC TEST LOADS AND DEFLECTIONS BY IDENTIFICATION

Consider the beam-type specimen used in these experiments in a "maneuver" producing 3 g's at station 0.5 and 2 g's at station 6.0 from external forces at stations 35.5 and 61.0. Taking the rigid-body acceleration coefficient submatrix, E, determined for shaking at station 0.5 and using five modes relating accelerations at stations 0.5 and 6 to external forces at stations 35.5 and 61.0, we find maneuver trim forces of -284.787 pounds at station 35.5 and 353.472 pounds at station 61.0. In actual practice, of course, the maneuver trim forces and moments would be given.

We take the free-body influence coefficient matrix for five modes shaking the specimen at station 0.5 and postmultiply by the external forces to obtain the maneuver deflections relative to inertial axes:

| Station | Deflections |
|---------|-------------|
| 0.5 in. | $7.135 \times 10^{-2}$ in. |
| 6 in. | $4.888 \times 10^{-2}$ in. |
| 25 in. | $-3.846 \times 10^{-2}$ in. |
| 35.5 in. | $-6.234 \times 10^{-2}$ in. |
| 61 in. | $7.510 \times 10^{-3}$ in. |
| 72.5 in. | $4.279 \times 10^{-2}$ in. |

Let us now suppose that we wished to suspend this specimen at stations 25.0 and 61.0 in a static strength test. We transform the deflections to be relative to zero deflection at the suspension stations and obtain:

| Station | Deflections |
|---------|-------------|
| 0.5 in. | .1517 in. |
| 6 in. | .1198 in. |
| 35.5 in. | $-4.184 \times 10^{-2}$ in. |
| 72.5 in. | $-1.5608 \times 10^{-2}$ in. |

Using only four modes in our system identification data reduction, we obtain the following deflections.

| Station | Deflections |
|---------|-------------|
| 0.5 in. | .1516 in. |
| 6 in. | .1199 in. |
| 35.5 in. | $-4.165 \times 10^{-2}$ in. |
| 72.5 in. | $-1.550 \times 10^{-2}$ in. |

These are the deflections, relative to zero at stations 25 and 61, which occur in the "maneuver" for 3 g's at station 0.5 and 2 g's at station 6.0.

We now wish to know what forces to apply to the static beam, suspended at stations 25 and 61, to produce the above deflections occurring in the maneuver. We transform the free-body inertial coefficient matrix to a static influence oefficient matrix for constraints at stations 25 and 61, and multiply the inverse of the SIC by the maneuver deflections.

With an FIC matrix formed by shaking at station 0.5 and covering five modes, we find the forces to be applied in the static test to be -3.485 pounds, 100.051 pounds, -317.75 pounds and 278.902 pounds. Using only four modes the forces calculation yields forces f 11.536 pounds, 78.620 pounds, -326.085 pounds and 200.557 pounds.

Although the accuracy with which the concentrated forces are determined is, as one would expect, not as good as the accuracy in the static deflections, it promises to be a substantial improvement over the arbitrariness of the present method of using judgment and intuition to approximate distributed inertial forces with a small number of concentrated forces.

This technique can be extended to approximating distributed
inertial static forces by many more concentrated forces than
modes covered in the system identification testing through
the use of Moore's Generalized Inverse of the SIC matrix.
Experimental investigation of this is beyond the scope of
the work of this report.  Nonsingular SIC matrices from
system identification will generally satisfy the requirements
of the present state of the art of static strength testing of
helicopters.

The static deflections occurring under maneuver do not involve
matrix inversion in their determination and are dominated by
the lower modes.  The engineer can determine the static de-
flection under maneuver g-loading by system identification
for every station at which he has an accelerometer and will
find, as shown, that very few modes need be covered for high
accuracy.

## IDENTIFIED STATIC INFLUENCE COEFFICIENTS

Consider the specimen pinned to "ground" at the 6-inch and
25-inch stations.  We wish to determine the static influence
coefficients among the 35.5-inch, the 61-inch, and the 72.5-
inch stations.

Using Bernoulli-Euler beam theory on the specimen, we
calculate the following matrix of static influence
coefficients.

$$\begin{bmatrix} 1.071 & & \text{Symmetric} \\ 4.239 & 24.21 & \\ 5.664 & 34.52 & 51.05 \end{bmatrix} \quad \frac{\text{in.}}{\text{lb}} \times 10^4$$

From test data obtained by shaking at the 72.5-inch station, we identified the following matrix of static influence coefficients.

$$\begin{bmatrix} 1.057 & & \text{Symmetric} \\ 4.036 & 29.90 & \\ 4.976 & 41.74 & 60.24 \end{bmatrix} \quad \frac{\text{in.}}{\text{lb}} \times 10^4$$

From test data obtained by shaking at the 0.5-inch station, we identified the following matrix of static influence coefficients.

$$\begin{bmatrix} 1.076 & & \text{Symmetric} \\ 4.139 & 26.43 & \\ 5.524 & 38.30 & 57.63 \end{bmatrix} \quad \frac{\text{in.}}{\text{lb}} \times 10^4$$

## MOBILITY RERUNS

An important proof of the value of a mathematical model is its ability to reproduce actual test data. The identified mathematical models were used to obtain mobility data, and Figures 10 through 25 show the comparisons between the actual mobility test data and the mobility plots given by the identified models. The situation here is not as simple as merely comparing a fitted curve to input points, although they are related, as failures of other methods of system identification to do so indicate (Reference 6). The problem is to construct a mathematical model of a limited number of degrees of freedom using modal parameters, deter- mined through testing, such that the identified mathematical model will accurately yield not only the modal response put into it, but the responses at frequencies removed from the natural frequencies. In other words, it is important for an identified mathematical model to be able to predict the interaction among modes.

The solid curves in Figures 10 through 25 show the predictions of the identified mathematical models while the circles show actual measurements. Note that the model identified by shaking at one end of the unsymmetrical specimen predicts a response from shaking at the other end of the specimen which accurately compares throughout the useful frequency range with actual test data obtained by shaking at the other end.
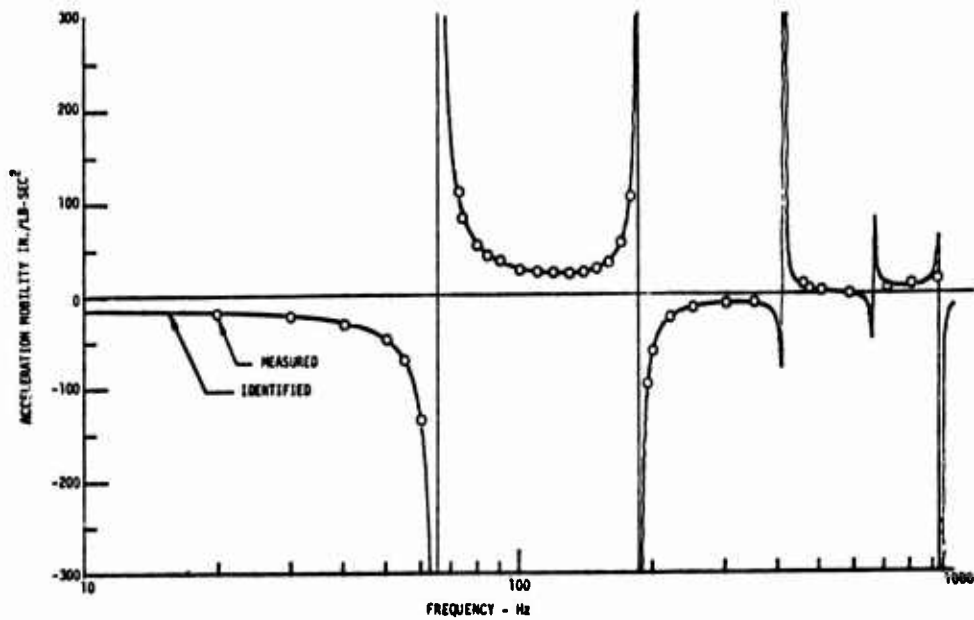
Figure 10.  Acceleration Mobility for Response at the 6-Inch
Station and Force at the 72.5-Inch Station.
Identification Made from Data Obtained With the
Force at the 72.5-Inch Station.



Figure 11.  Acceleration Mobility for Response at the 25-Inch
Station and Force at the 72.5-Inch Station.
Identification Made from Data Obtained With the
Force at the 72.5-Inch Station.

63

Figure 12. Acceleration Mobility for Response at the 35.5-Inch Station and Force at the 72.5-Inch Station. Identification Made from Data Obtained With the Force at the 72.5-Inch Station.



Figure 13. Acceleration Mobility for Response at the 61-Inch Station and Force at the 72.5-Inch Station. Identification Made from Data Obtained With the Force at the 72.5-Inch Station.
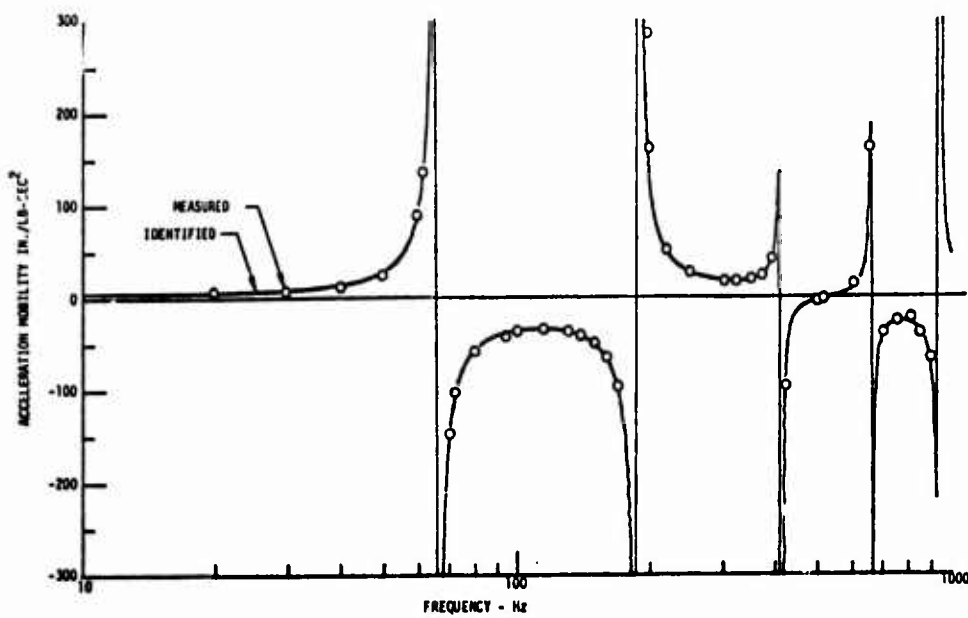
Figure 14.    Acceleration Mobility for Response at the 72.5-Inch Station and Force at the 72.5-Inch  tation. Identification Made from Data Obtained With the Force at the 72.5-Inch Station.
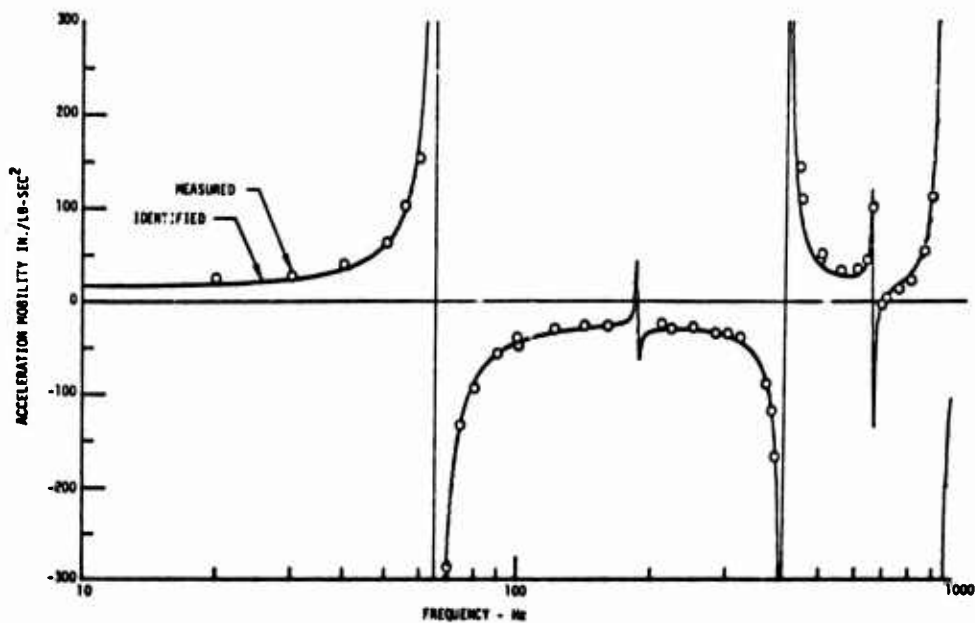


Figure 15.    Acceleration Mobility for Response at the 6-Inch Station and Force at the 72.5-Inch Station. Identification Made from Data Obtained With the Force at the 0.5-Inch Station.

Figure 16.   Acceleration Mobility for Response at the 25-Inch
Station and Force at the 72.5-Inch Station.
Identification Made from Data Obtained With the
Force at the 0.5-Inch Station.



Figure 17.   Acceleration Mobility for Response at the 35.5-
Inch Station and Force at the 72.5-Inch Station.
Identification Made from Data Obtained With the
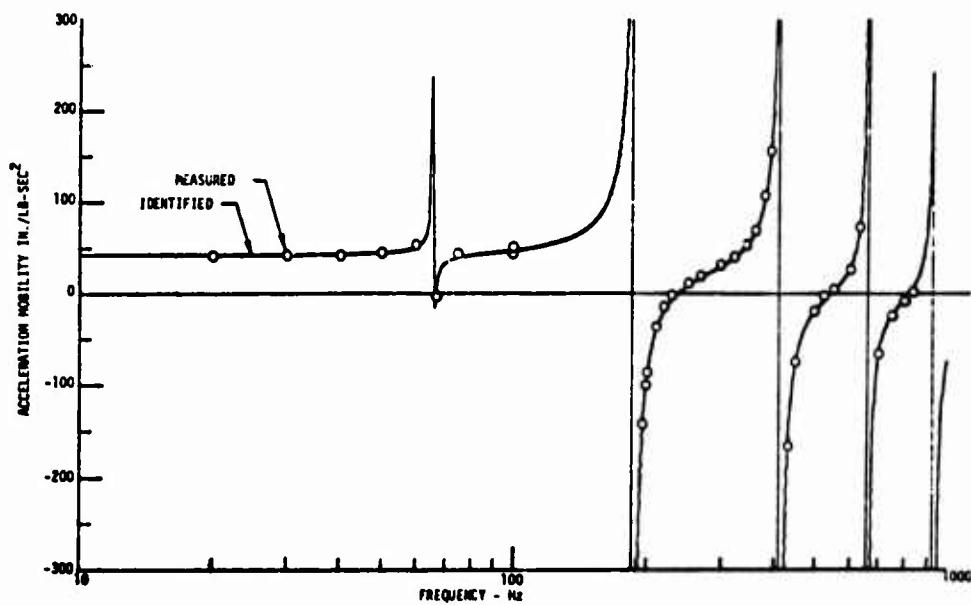Force at the 0.5-Inch Station.

Figure 18. Acceleration Mobility for Response at the 61-Inch Station and Force at the 72.5-Inch Station. Identification Made from Data Obtained With the Force at the 0.5-Inch Station.
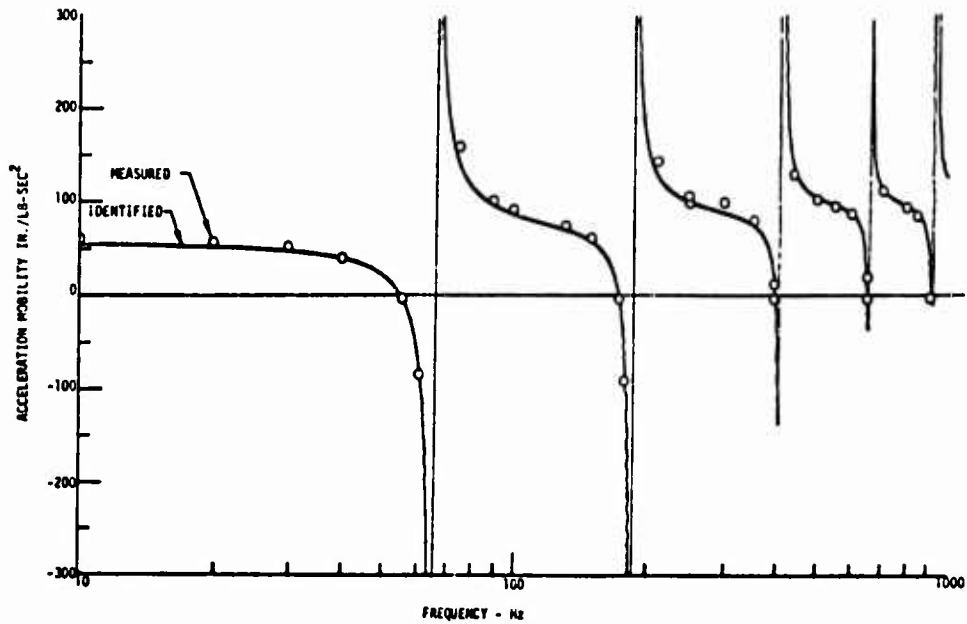


Figure 19. Acceleration Mobility for Response at the 72.5-Inch Station and Force at the 72.5-Inch Station. Identification Made from Data Obtained With the Force at the 0.5-Inch Station.
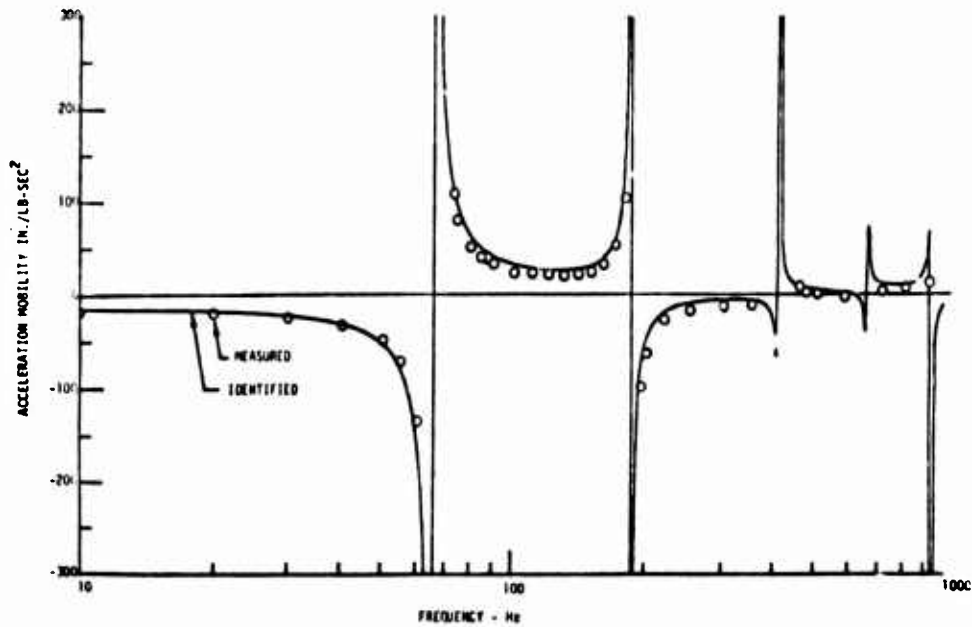
67
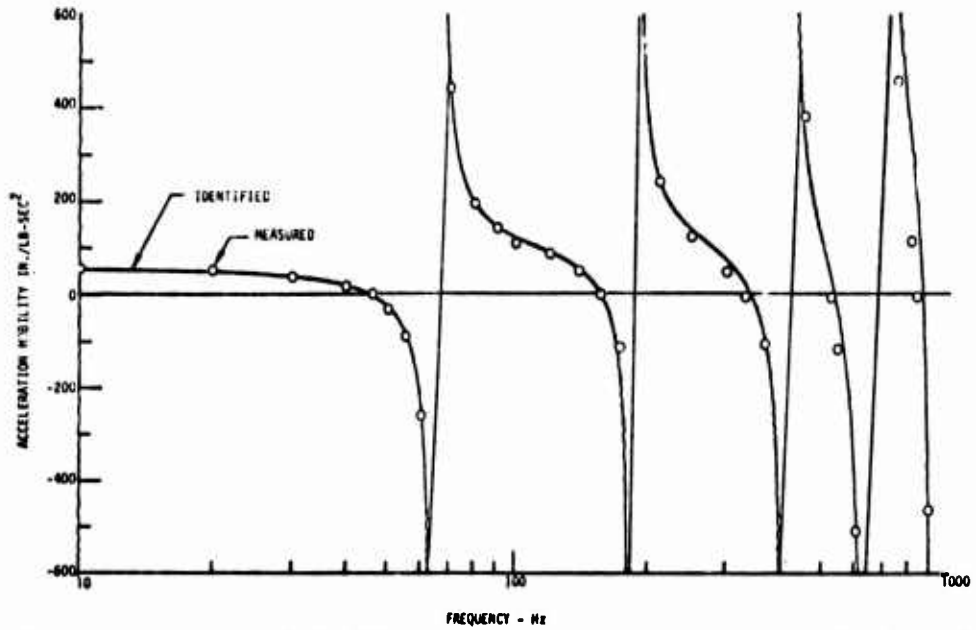
Figure 20.  Acceleration Mobility for Response at the 0.5-Inch
Station and Force at the 0.5-Inch Station.
Identification Made from Data Obtained With the
Force at the 0.5-Inch Station.
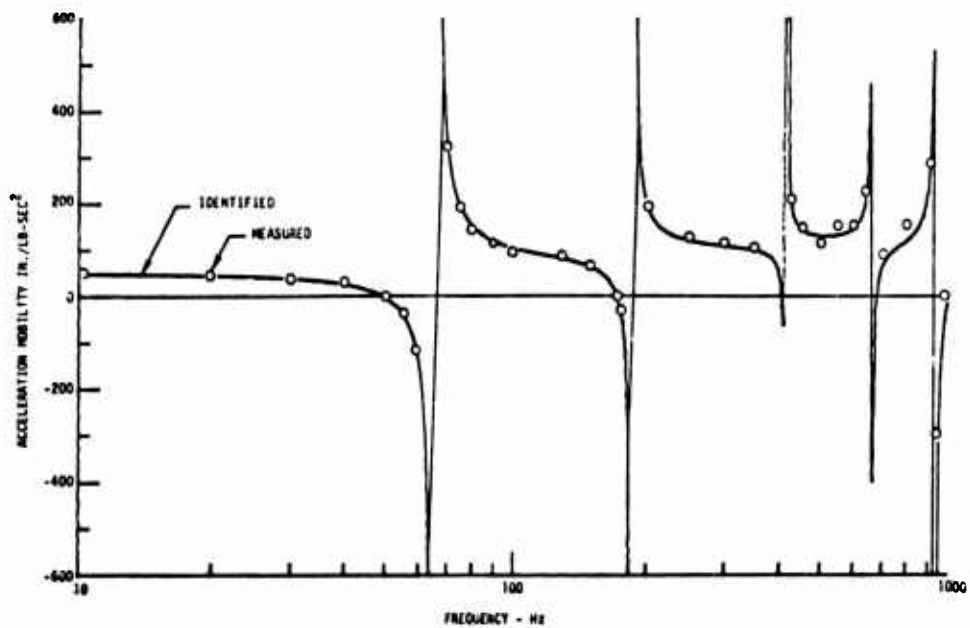


Figure 21.  Acceleration Mobility for Response at the 6-Inch
Station and Force at the 0.5-Inch Station.
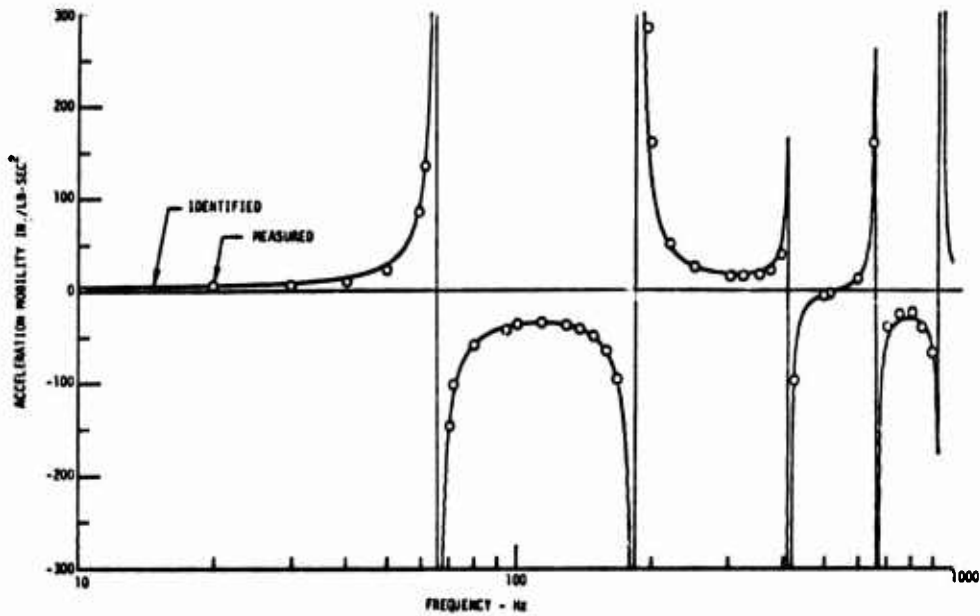Identification Made from Data Obtained With the
Force at the 0.5-Inch Station.
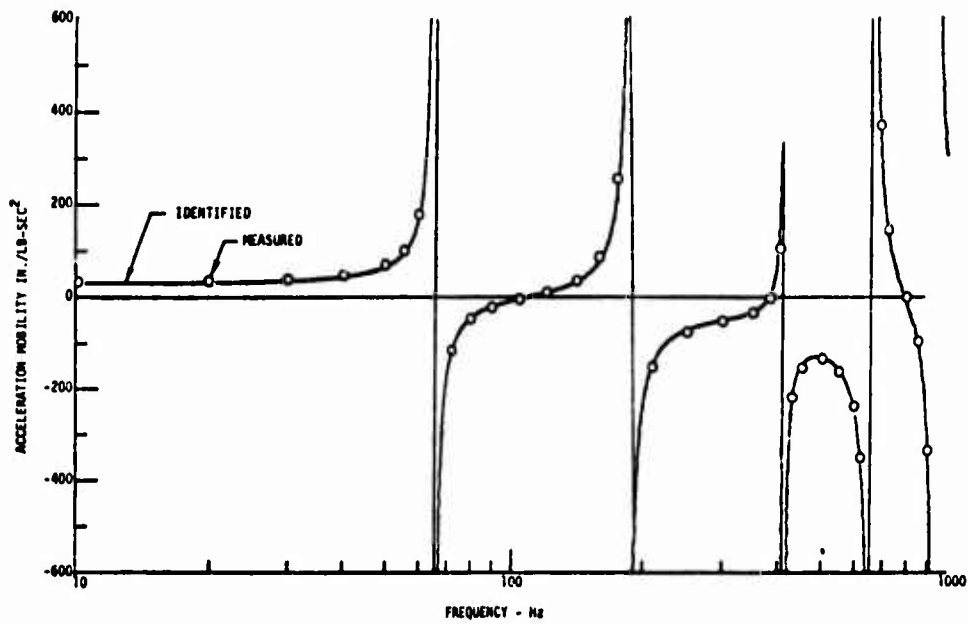
Figure 22. Acceleration Mobility for Response at the 25-Inch Station and Force at the 0.5-Inch Station. Identification Made from Data Obtained With the Force at the 0.5-Inch Station.
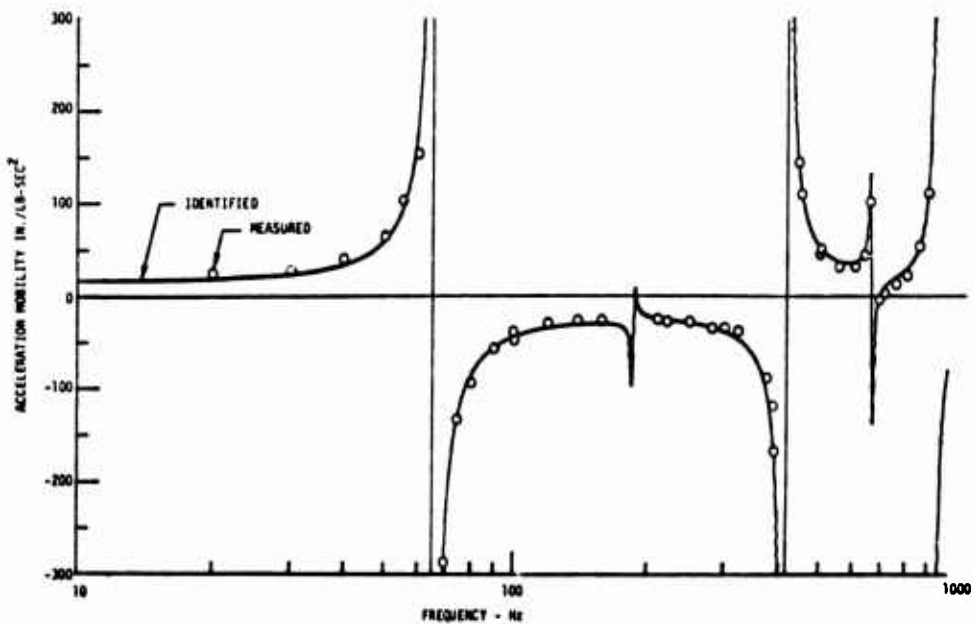


Figure 23. Acceleration Mobility for Response at the 35.5-Inch Station and Force at the 0.5-Inch Station. Identification Made from Data Obtained With the Force at the 0.5-Inch Station.
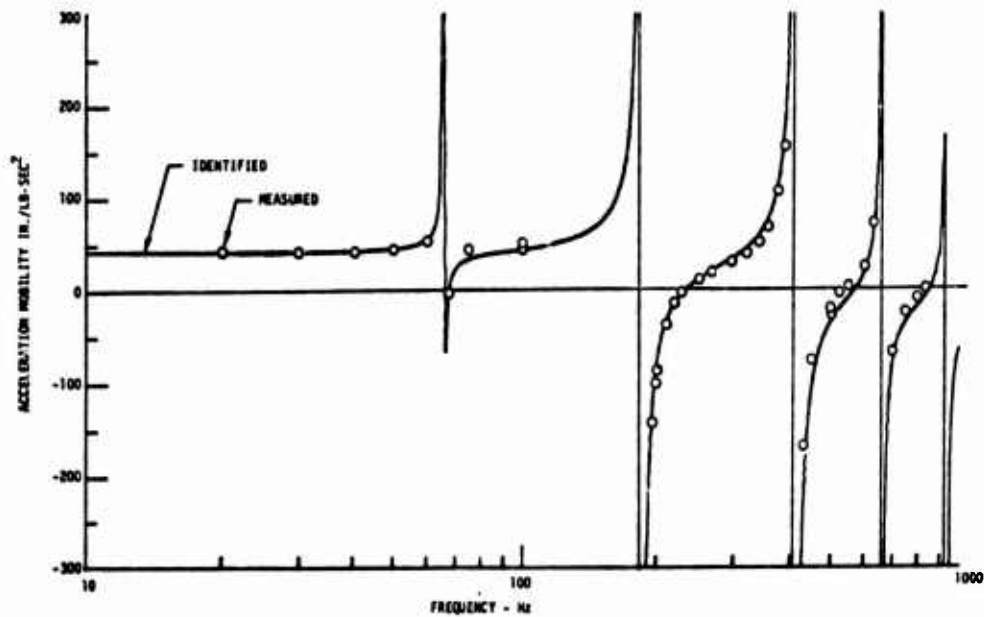
Figure 24. Acceleration Mobility for Response at the 61-Inch Station and Force at the 0.5-Inch Station. Identification Made from Data Obtained With the Force at the 0.5-Inch Station.
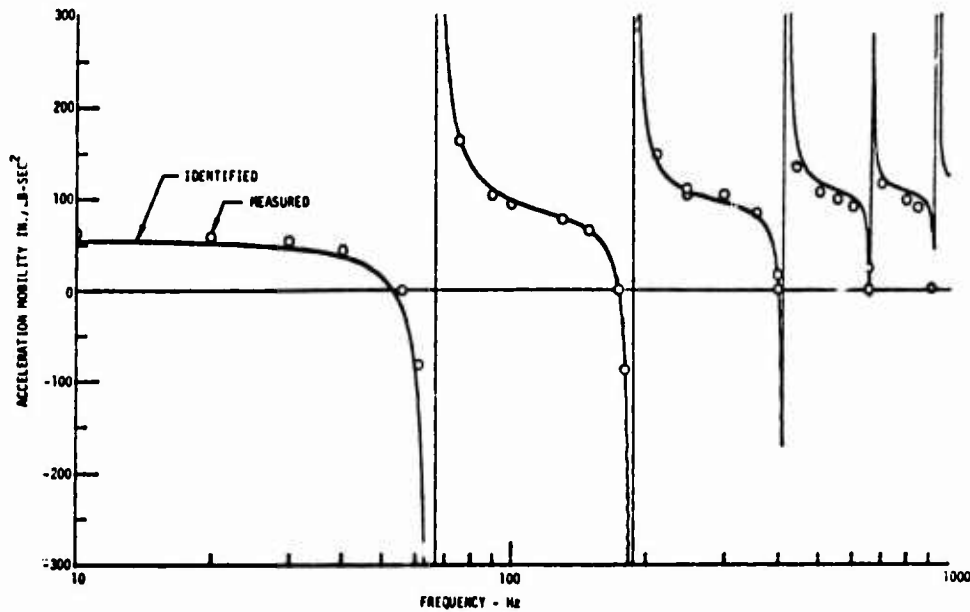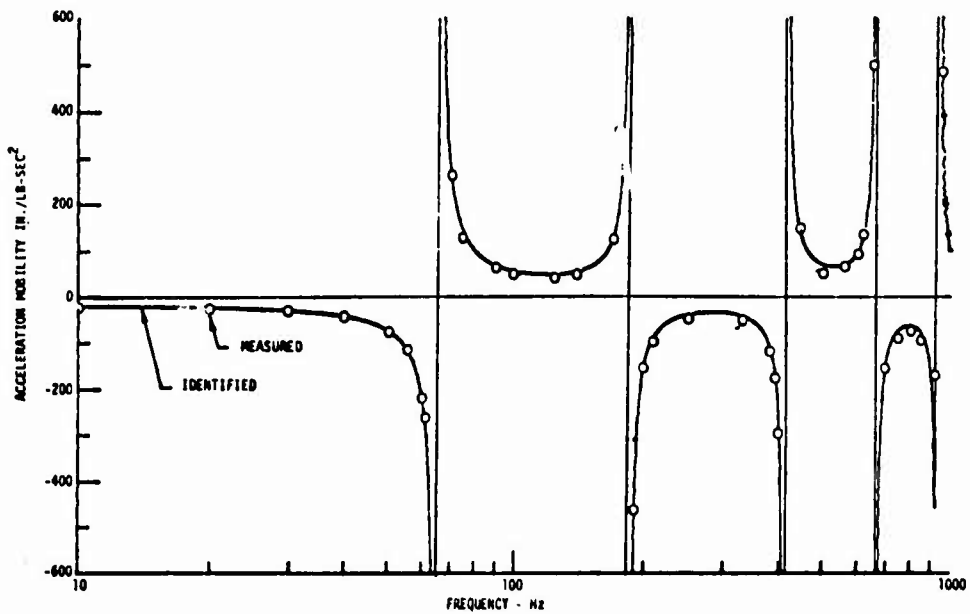


Figure 25. Acceleration Mobility for Response at the 72.5-Inch Station and Force at the 0.5-Inch Station. Identification Made from Data Obtained With the Force at the 0.5-Inch Station.
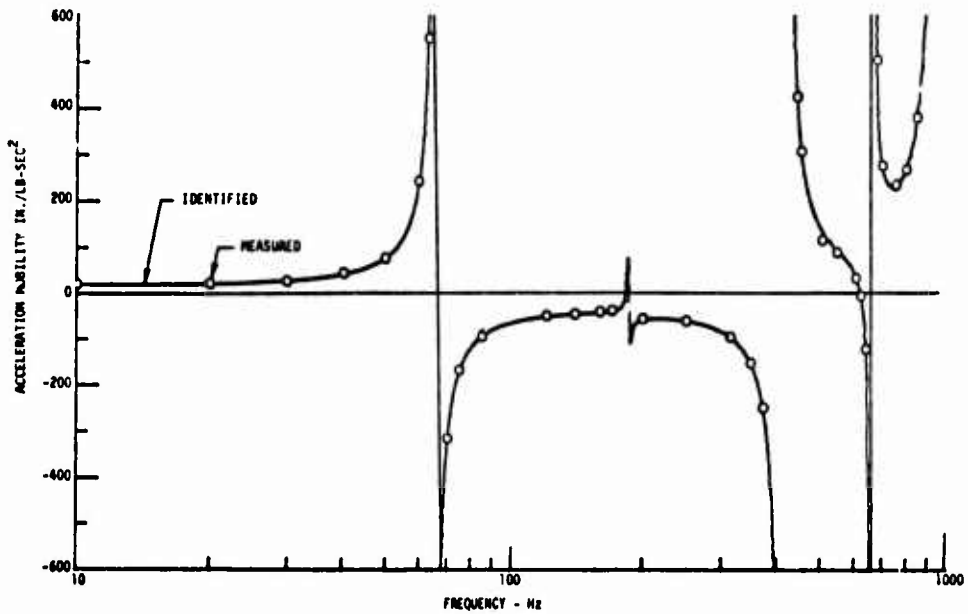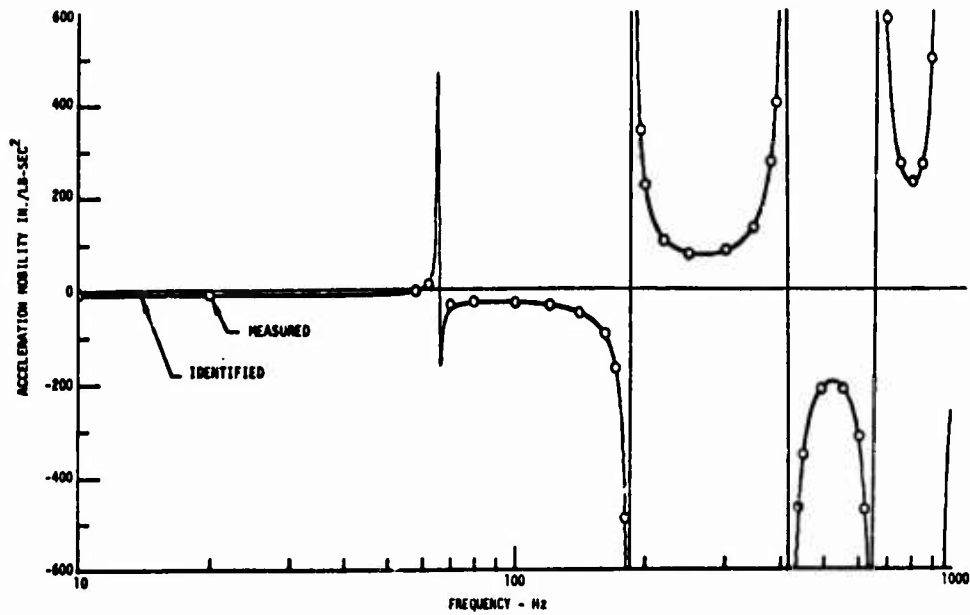
70

# CONCLUSIONS

1. The laboratory testing confirmed that it is possible to accurately identify the properties of a continuous asymmetric structure through single-point shaking impedance-type testing.

2. It was found by laboratory experiments that it is possible to obtain static influence coefficients for arbitrary restraint through free-body testing without assumption of a mass matrix.

3. It was found by laboratory experiments that the equations of Biot and Duncan, slightly modified, can be validly used in the presence of imaginary antiresonances.

4. It was found by laboratory experiments that normal modes and modal masses can be determined accurately from test data by an antiresonance theory equation with single-point shaking on structures of ordinary levels of structural damping without use of matrix inversion.

5. It was found by laboratory experiments that iteration to determine modal parameters by matrix methods is not necessary with low damping.

6. Identification of a model with more degrees of freedom than modes covered in the testing (truncated model) was found to be accurate, in the laboratory experiments.

7. Truncated models can be used to predict the effects of stiffness and mass changes.

8. It was found by laboratory experiments that free-body influence coefficients may be expressed as a function of only the rigid body acceleration coefficient, the natural frequencies and the antiresonant frequencies.

9. The equations of Duncan and Biot were extended to free systems and found to be valid.

10. Maneuver inertial loads of the distributed helicopter structure can be lumped for static testing by system identification methods.

11. It was found by laboratory experiments that impedance test data should not be relied on unless physical checks, independent of the signals and transducers, are made during the testing.

71

## RECOMMENDATIONS

1. The application of system identification by the method of these laboratory experiments to a large semimonocoque structure, such as a tail boom or full fuselage, should be investigated by testing in a manner that will define the proper and necessary procedures for general helicopter engineering use.

2. Application of these methods to solving the problems of the dynamics of main and tail rotor blades should be investigated, with particular attention to the structural properties of elastically articulated blades.

3. The new approaches to dynamic testing offered by antiresonance theory should be further expanded to allow widespread on-site application of hand-calculator or computer terminal checking of data during helicopter shake testing and physically meaningful instant reduction of data to the modal, static, and inertial properties required.

# LITERATURE CITED

1. Kenigsberg, I. J., CH-53A FLEXIBLE FRAME VIBRATION ANALYSIS/TEST CORRELATION, Sikorsky Aircraft Corp., Final Report, Contract N00019-72-C-0411, Department of the Navy, Naval Air Systems Command, 28 March 1973.

2. Seaholm, N. A., and Sodergren, J. H., SUBSTRUCTURING TECHNIQUES AND THEIR IMPACT ON DYNAMIC TEST REQUIRE-MENTS, Symposium on Substructure Testing and Synthesis, Marshall Space Flight Center, 30 August 1972.

3. Vance, J. M., DYNAMIC COMPATIBILITY OF ROTARY-WING AIRCRAFT PROPULSION COMPONENTS, USAAMRDL Technical Report 73-10, Eustis Directorate, U. S. Army Air Mobility Research and Development Laboratory, Fort Eustis, Virginia, January 1973, AD 761100.

4. Yaggy, P. F., THE OLD BAG OF EMPIRICISM IS BARE, Guest Editorial, Vertiflite, Vol. 20, No. 2, March/April 1974.

5. Flannelly, W. G., Berman, A., and Giansante, N., RESEARCH ON STRUCTURAL DYNAMIC TESTING BY IMPEDANCE METHODS, VOLUME II - STRUCTURAL SYSTEM IDENTIFICATION FROM SINGLE-POINT EXCITATION, Kaman Aerospace Corporation, USAAMRDL Technical Report 72-63B, Eustis Directorate, U. S. Army Air Mobility Research and Development Laboratory, Fort Eustis, Virginia, November 1972, AD 756390.

6. Flannelly, W. G., and Berman, A., THE STATE OF THE ART OF SYSTEM IDENTIFICATION OF AEROSPACE STRUCTURES, 1972 Winter Annual Meeting of the American Society of Mechanical Engineers, New York, November 1972.

7. Rodden, W. P., A METHOD FOR DERIVING STRUCTURAL INFLUENCE COEFFICIENTS FROM GROUND VIBRATION TESTS, AIAA Journal, Vol. 5., No. 5, May 1967.

8. Kennedy, C. C., and Pancu, C. D. P., USE OF VECTORS IN VIBRATION MEASUREMENT AND ANALYSIS, J. Aero. Sciences, Vol. 14, No. 11, November 1947.

9. Biot, M. A., COUPLED OSCILLATIONS OF AIRCRAFT-ENGINE PROPELLER SYSTEMS, J. Aero. Sciences, Vol. 7, No. 9, July 1940.

10. Duncan, W. J., MECHANICAL ADMITTANCE AND THEIR APPLICA-
    TIONS TO OSCILLATION PROBLEMS, Aeronautical Research
    Council R&M No. 2000 (monograph), London: His Majesty's
    Stationary Office, 1947.

11. Bishop, R. E. D., and Johnson, D. C., THE MECHANICS OF
    VIBRATION, Cambridge, at the University Press, 1960.

12. Klosterman, A. L., DETERMINATION OF DYNAMIC INFORMATION
    BY USE OF VECTOR COMPONENTS OF VIBRATION, University
    of Cincinnati, 1968.

13. Stahle, C. V., PHASE SEPARATION TECHNIQUE FOR GROUND
    VIBRATION TESTING, Aerospace Engineering, July 1962.

14. Berman, A., and Flannelly, W. G., THEORY OF INCOMPLETE
    MODELS OF DYNAMIC STRUCTURES, AIAA Journal, Vol. 9,
    No. 8, August 1971.

# APPENDIX A
## TRUNCATED MODELS AND THEIR USE IN PREDICTING
## EFFECTS OF CHANGES IN MASS AND STIFFNESS

## SUMMARY

Truncated parameters of a linear system are defined herein
as those constant matrix coefficients in the equations of
motion formed from fewer normal modes than degrees of freedom
such that the Euclidian norm of the differences between the
actual mobility matrix and the mobility matrix formed using
the normal modes and modal coefficients of the parameters is
a minimum with respect to the modal coefficients. An engineer
can construct a truncated mathematical model of a linear
system from fewer normal modes than degrees of freedom in
the system.

It is shown that the classical dynamical eigenvalue problem
using truncated influence coefficient and mass matrices
yields as many normal modes and natural frequencies, exactly,
as the column rank of the normal mode matrix used in forming
the truncated parameters. It is further shown that truncated
mathematical models can be used to predict the effects of
mass and stiffness changes to the extent that the new dynami-
cal eigenvectors can be expressed as linear combinations of
the original dynamical eigenvectors and this is demonstrated
via computer experiments.

## DERIVATION OF TRUNCATED MODELS OF LINEAR STRUCTURES AND
## PREDICTION OF CHANGES IN MASS AND STIFFNESS

As shown in Reference 1, the mobilities of J coordinates for
excitation at coordinate k is given by

$$\{Y_{j(k\omega)}\} = [\Phi][\phi_{(k)i}]\{Y^*_{i(\omega)}\} + \{\delta\}$$

$$\text{Jx1} \qquad \text{JxN} \quad \text{NxN} \quad \text{Nx1} \quad \text{Jx1}$$

(A-1)

where $\{\delta\}$ is the difference between the actual mobility and
that approximated using only N modes. For the full mobility
matrix this becomes

$$[Y_{jk(\omega)}] = [\Phi][Y^*_{i(\omega)}][\Phi]^T + [\delta]$$

$$\text{JxJ} \qquad \text{JxN} \quad \text{NxN} \quad \text{NxJ} \quad \text{JxJ}$$

(A-2)

Using Equation (A-1) we set the partial derivative of $\{\delta\}^T\{\delta\}$ with respect to $\{Y^*_{i(\omega)}\}$ equal to zero and solve for the modal mobility vector which will make the Euclidian norm of the residuals, $\{\delta\}$, a minimum.

$$[\phi_{(k)i}]\{Y^{*\prime}_{i(\omega)}\} = [Y^{*\prime}_{i(\omega)}]\{\phi_{(k)i}\} = [\phi]^+\{Y_{j(k\omega)}\} \qquad (A-3)$$

where $[\phi]^+ \equiv ([\phi]^+[\phi])^{-1}[\phi]^T$. For the full mobility matrix of Equation (A-2), Equation (A-3) can be immediately extended to give the minimum Euclidian norm of $[\delta]$.

$$[Y^{*\prime}_{i\omega}] = [\phi]^+[Y_{jk(\omega)}][\phi]^{+T} \qquad (A-4)$$

The truncated mobility matrix is now defined as

$$[Y]_T \equiv [\phi][\phi]^+[Y][\phi]^{+T}[\phi]^T \qquad (A-5)$$

and the Truncated Impedance matrix as

$$[Z]_T = [\phi]^{+T}[\tfrac{1}{Y^{*\prime}}][\phi]^+ \qquad (A-6)$$

Note that

$$[\phi]^+[Y]_T[Z]_T[\phi] = I \qquad (A-7)$$

and

$$[\phi]^T[Z]_T[Y]_T[\phi]^{+T} = I \qquad (A-8)$$

We define the Truncated Stiffness as

$$[K]_T = [\phi]^{+T}[K^*_i][\phi]^+ \qquad (A-9)$$

the Truncated Mass as

$$[m]_T = [\phi]^{+T}[M^*_i][\phi]^+ \qquad (A-10)$$

76

and the Truncated Influence Coefficient, in the manner of Rodden (Reference 2 ) and Berman (Reference 3 ), as

$$[C]_T = [\phi][\frac{1}{K_i^*}][\phi]^T \qquad (A-11)$$

If the truncated modal mobilities of Equation (A-6) are very nearly equal to the actual modal mobilities (which they will usually be if modal matrix contains the three or four modes in the vicinity of the forcing frequency), we can use the modal mobilities in Equation (A-6) and will obtain Equations (A-9) and (A-10) by, respectively, setting the forcing frequency to zero and infinity. Similarly, Equation (A-11) can be obtained from Equation (A-5) by setting the forcing frequency to zero.

Premultiplying Equation (A-10) by Equation (A-11) gives the classical eigenvalue equation using truncated parameter matrices:

$$[C]_T[m]_T[\phi] = [\phi][\frac{1}{\Omega^2}] \qquad (A-12)$$

as shown in Reference 1.

We may rewrite Equation (A-1) as

$$\{Y_{j(k\omega)}\} \underset{JxN}{\cong} [\phi]\{q\}$$

or, for velocity

$$\{\tilde{\dot{y}}\} = \{Y_{j(k\omega)}\}\tilde{f}_k \cong [\phi] \{\dot{q}\} \qquad (A-13)$$
$$\underset{JxN \ Nx1}{}$$

From Equation (A-10) we see that the Kinetic Energy is

$$T = \frac{1}{2}\{\dot{y}\}^T[m]\{\dot{y}\} = \frac{1}{2}\{\dot{q}\}^T[\phi]^T[m] \quad [\phi] \quad \{\dot{q}\}$$
$$\underset{1xN \ NxJ \ JxJ \ JxN \ Nx1}{}$$

$$= \frac{1}{2}\{\dot{q}\}^T[M^*]\{\dot{q}\} = \frac{1}{2}\{\dot{q}\}^T[\phi]^T[m]_T[\phi]\{\dot{q}\} \qquad (A-14)$$
$$\underset{NxN}{}$$

Consider a change in the mass and in the stiffness such that the new displacements in the frequency range of interest are approximated by a linear combination of the original N modes.

$$\{\dot{y}\} = [\Phi] \quad \{r\}$$
$$\text{Jx1} \quad \text{JxN} \quad \text{Nx1}$$

(A-15)

The new kinetic energy is approximated by

$$T \stackrel{\sim}{=} \frac{1}{2} \{\dot{r}\}^T [\Phi]^T ([m] + [\Delta m]) [\Phi] \{\dot{r}\}$$

(A-16)

But

$$[\Phi]^T [m] \quad [\Phi] = [\Phi]^T [m]_T [\Phi] = [M^*]$$
$$\text{NxJ} \quad \text{JxJ} \quad \text{JxN} \quad \quad \quad \quad \text{NxN}$$

and

$$[\Phi]^T [\Delta m] [\Phi] = [\Phi]^T ([\Phi]^{+T} [\Phi]^T [\Delta m] [\Phi] [\Phi]^+) [\Phi] = [\Phi]^T [\Delta m]_T [\Phi]$$

(A-17)

Defining $[\Delta m]_T \equiv [\Phi]^{+T} [\Phi]^T [\Delta m] [\Phi] [\Phi]^+$, the kinetic energy becomes

$$T \cong \frac{1}{2} \{\dot{r}\}^T [\Phi]^T ([m]_T + [\Delta m]_T) [\Phi] \{\dot{r}\}$$

(A-18)

Similarly, the potential energy is found to be

$$V \cong \frac{1}{2} \{r\}^T [\Phi]^T ([K] + [\Delta K]) [\Phi] \{r\} = \frac{1}{2} \{r\}^T [\Phi]^T ([K]_T$$
$$+ [\Delta K]_T) [\Phi] \{r\}$$

(A-19)

where

$$[\Delta K]_T = [\Phi]^{+T} [\Phi]^T [\Delta K] [\Phi] [\Phi]^+$$

(A-20)

Note that $[\Phi]^T [\Delta m] [\Phi]$ and $[\Phi]^T [\Delta K] [\Phi]$ are not ordinarily diagonal.

78

As seen from Equations (A-9) and (A-11), the new truncated influence coefficient matrix is given by

$$[C']_T = [\phi] \quad [\phi]^T ([K]_T + [\Delta K]_T) [\phi]^{-1} [\phi]^T \quad (A-21)$$

and the eigenvalue equation reflecting the changes is

$$[C']_T [m']_T [\phi'] = [\phi'] [\frac{1}{\Omega'^2}] \quad (A-22)$$

where the new eigenvectors are linear combinations of the original eigenvectors:

$$[\phi'] \{S\} = \{y\} = [\phi] \{r\}$$

Computer experiments were run on the Hewlett Packard 2000C computer using, as a specimen, an elastically supported beam of irregular continuous stiffness and ten unequal lumped masses totaling 9200 pounds.

The mass changes shown in Tables A-1 and A-2 consisted of raising the mass of the first station from 11.2 pounds to 22.4 pounds and increasing the mass of the second station from 2840 pounds to 4260 pounds. The stiffness change of Tables A-3 and A-4 was effected by doubling the stiffness between stations 2 and 3; i.e., adding a spring between coordinates 2 and 3 of rate 374,000 pounds/inch.

Only the first three modes of the unchanged system were used in constructing the truncated model from Equations (A-9), (A-10), and (A-11). The natural frequencies and mode shapes of the system with changes were calculated using Equation (A-22).

The stiffness change was more drastic than the mass changes and it will be noted in Tables A-3 and A-4 that although the change severely altered the first and second mode shapes, the truncated model predicted the new frequencies and mode shapes quite accurately.

79

| TABLE A-1. EFFECT OF MASS CHANGES ON THE FIRST MODE AND PREDICTED EFFECT FROM TRUNCATED MODEL | | |
|---|---|---|
| Mode I | | |
| Exact Solution No Changes | Exact Solution With 100% Change in Mass 1 & 50% Change in Mass 2 | 3 Mode Truncated Solution With 100% Change in Mass 1 & 50% Change in Mass 2 |
| Nat Freq 3.45067 cps | 3.18247 cps | 3.18257 cps |
| Mode Shapes | | |
| 1 | 1 | 1 |
| .765 | .778 | .779 |
| .490 | .516 | .516 |
| .378 | .408 | .408 |
| .273 | .304 | .305 |
| .173 | .205 | .205 |
| .080 | .111 | .111 |
| -.006 | .023 | .024 |
| -.122 | -.100 | -.100 |
| -.235 | -.218 | -.218 |

| TABLE A-2. EFFECT OF MASS CHANGES ON THE SECOND MODE AND PREDICTED EFFECT FROM TRUNCATED MODEL | | |
|---|---|---|
| **Mode II** | | |
| Exact Solution No Changes | Exact Solution With 100% Change in Mass 1 & 50% Change in Mass 2 | Truncated Solution Using Only 3 Modes With 100% Change in Mass 1 & 50% Change in Mass 2 |
| Nat Freq 9.68024 cps | 8.49711 cps | 8.49895 cps |
| **Mode Shapes** | | |
| 1 | 1 | 1 |
| .397 | .450 | .452 |
| -.253 | -.136 | -.137 |
| -.465 | -.327 | -.328 |
| -.642 | -.483 | -.486 |
| -.782 | -.608 | -.613 |
| -.881 | -.697 | -.703 |
| -.938 | -.748 | -.755 |
| -.954 | -.763 | -.768 |
| -.968 | -.770 | -.771 |

| TABLE A-3. EFFECT OF STIFFNESS CHANGE ON THE FIRST MODE AND PREDICTED EFFECT FROM TRUNCATED MODEL | | |
|---|---|---|
| Mode I | | |
| Exact Solution No Changes | Exact Solution Double Stiffness Between Sta 2 & 3 | 3 Mode Truncated Solution Double Stiffness Between Sta 2 & 3 |
| Nat Freq 3.45067 cps | 8.14744 cps | 8.22313 cps |
| Mode Shapes | | |
| 1 | 1 | 1 |
| .765 | .524 | .533 |
| .490 | .031 | .032 |
| .378 | -.113 | -.130 |
| .273 | -.232 | -.266 |
| .173 | -.330 | -.376 |
| .08 | -.404 | -.456 |
| -.006 | -.454 | -.505 |
| -.122 | -.490 | -.522 |
| -.235 | -.519 | -.519 |

| TABLE A-4. | EFFECT OF STIFFNESS CHANGE ON THE SECOND MODE AND PREDICTED EFFECT FROM TRUNCATED MODEL | |
| --- | --- | --- |
| Mode II | | |
| Exact Solution No Changes | Exact Solution Double Stiffness Between Sta 2 & 3 | 3 Mode Truncated Solution Double Stiffness Between Sta 2 & 3 |
| Nat Freq 9.68024 cps | 16.8013 cps | 16.9646 cps |
| Mode Shapes | | |
| 1 | +.381 | .256 |
| .397 | +.180 | .140 |
| -.253 | .104 | .082 |
| -.465 | .198 | .122 |
| -.642 | .306 | .179 |
| -.782 | .413 | .249 |
| -.881 | .515 | .334 |
| -.938 | .614 | .440 |
| -.954 | .774 | .662 |
| -.968 | 1 | 1 |

# REFERENCES

1. Flannelly, W. G., Giansante, N., and Berman, A., SYSTEM IDENTIFICATION WITH EXCITATION OF ONE DEGREE OF FREEDOM, Kaman Aerospace Corporation Research Note 71-1, Kaman Aerospace Corporation, Bloomfield, Connecticut, 18 February 1971.

2. Berman, A., and Flannelly, W. G., THEORY OF INCOMPLETE MODELS OF DYNAMIC STRUCTURES, AIAA Journal, Volume 9, No. 8, pp. 1481-1487, August 1971.

3. Rodden, W. P., A METHOD FOR DERIVING STRUCTURAL INFLUENCE COEFFICIENTS FROM GROUND VIBRATION TESTS, AIAA Journal, Volume 5, No. 5, pp. 991-1000, May 1967.

4. Ross, R. G., SYNTHESIS OF STIFFNESS AND MASS MATRICES FROM EXPERIMENTAL VIBRATION MODES, SAE Paper 71087.

# APPENDIX B
## RIGID-BODY ACCELERATION COEFFICIENT FOR
## PRINCIPAL OR NONPRINCIPAL AXES

In Figure B-1 x, y, and z are any orthogonal axes through the center of gravity of a body of mass M, with points $x_i$, $y_i$, and $z_i$, shown on the respective axes, having rotational acceleration $\ddot{\theta}_x$, $\ddot{\theta}_y$, and $\ddot{\theta}_z$.
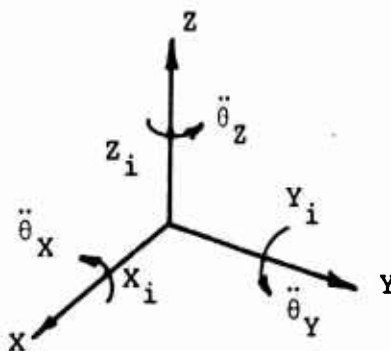


Figure B-1. Axis System.

The moments $M_x$, $M_y$, and $M_z$ about the x, y, and z axes, respectively, may be written using Lagrange's Equation as

$$\begin{Bmatrix} M_x \\ M_y \\ M_z \end{Bmatrix} = \begin{bmatrix} I_x & -U_{xy} & U_{xz} \\ -U_{xy} & I_y & -U_{zy} \\ -U_{xz} & -U_{zy} & I_z \end{bmatrix} \begin{Bmatrix} \ddot{\theta}_x \\ \ddot{\theta}_y \\ \ddot{\theta}_z \end{Bmatrix} \tag{B-1}$$

where $I_x$, $I_y$, and $I_z$ are the moments of inertia about the x, y, and z axes, respectively, and $U_{xy}$, $U_{xz}$, and $U_{zy}$ are the product of inertia with respect to the x and y axes, the x and z axes, and the y and z axes, respectively.

Equation (B-1) may be written in general notation as

$$\{M_q\} = [\partial M/\partial \ddot{\theta}]\{\ddot{\theta}\} \tag{B-2}$$

85

The $[\partial M/\ddot\theta]$ matrix may be inverted to yield

$$[\frac{\partial M}{\ddot\theta}]^{-1} \equiv [\frac{\ddot\theta}{\partial M}] = \frac{1}{\Delta} \begin{bmatrix} I_y I_z - U_{zy}^2 & U_{xy} I_z + U_{zy} U_{xz} & U_{xy} U_{zy} + I_y U_{xz} \\ U_{xy} I_z + U_{zy} U_{xz} & I_x I_z - U_{xz}^2 & I_x U_{zy} + U_{xy} U_{xz} \\ U_{xy} U_{zy} + I_y U_{xz} & I_x U_{zy} + U_{xy} U_{xz} & I_x I_y - U_{xy}^2 \end{bmatrix}$$

(B-3)

where $\Delta = I_x I_y I_z - 2U_{xy} U_{zy} U_{xz} - U_{xy}^2 I_z - U_{zy}^2 I_x$.

Solving for the rotational accelerations and using the definition presented in Equation (B-3) yields

$$\{\ddot\theta\} = [\frac{\ddot\theta}{\partial M}]\{M_q\}$$

(B-4)

The matrix $[\ddot\theta/\partial M]$ represents the rigid-body acceleration coefficients of the rotational acceleration about any of the specified axes with respect to a moment about any of the given axes.

The linear accelerations of the points $x_i$, $y_i$, and $z_i$ due solely to rotations of the rigid body may be expressed as

$$\begin{Bmatrix} \ddot{x}_i \\ \ddot{y}_i \\ \ddot{z}_i \end{Bmatrix} = \begin{bmatrix} 0 & z_i & -y_i \\ z_i & 0 & x_i \\ y_i & -x_i & 0 \end{bmatrix} \begin{Bmatrix} \ddot\theta_x \\ \ddot\theta_y \\ \ddot\theta_z \end{Bmatrix}$$

(B-5)

Equation (B-5) may be written more generally using Equation (B-4):

$$\{q\} = [Q_i]\{\ddot\theta\} = [Q_i][\partial\dot\theta/\partial M]\{M_q\}$$

(B-6)

The moments about the x, y, and z axes caused by orthogonal forces at any point are given by

$$
\begin{Bmatrix} M_x \\ M_y \\ M_z \end{Bmatrix} = \begin{bmatrix} 0 & -z_F & y_F \\ z_F & 0 & x_F \\ -y_F & x_F & 0 \end{bmatrix} \begin{Bmatrix} F_x \\ F_y \\ F_z \end{Bmatrix} \tag{B-7}
$$

Equation (B-7) may be written as

$$
\{M_q\} = [Q_F]\{F\} \tag{B-8}
$$

Newton's Law relates the accelerations of the center of gravity of the body to the applied forces and mass of the body:

$$
\{\ddot{q}_o\} = \begin{Bmatrix} \ddot{x}_o \\ \ddot{y}_o \\ \ddot{z}_o \end{Bmatrix} = \begin{Bmatrix} F_x \\ F_y \\ F_z \end{Bmatrix} \frac{1}{M} = \{F\} \frac{1}{M} \tag{B-9}
$$

The rigid-body acceleration coefficients describing rotational acceleration due to moment is given by Equation (B-3) and is written in matrix form as

$$
[\varepsilon_{\ddot{\theta}M}] = [\frac{\partial\ddot{\theta}}{\partial M}] \tag{B-10}
$$

The rigid-body acceleration coefficients relating translational acceleration and moment is obtained from Equation (B-6):

$$
[\varepsilon_{\ddot{q}M}] \equiv [\partial\ddot{q}/\partial M] = [Q_i][\partial\ddot{\theta}/\partial M] = [Q_i][\varepsilon_{\ddot{\theta}M}] \tag{B-11}
$$

The rigid-body acceleration coefficients presenting rotational acceleration due to force is defined from Equations (B-4) and (B-8):

$$[\varepsilon_{\ddot{\theta}F}] \equiv [\partial\ddot{\theta}/\partial F] = [\frac{\partial\ddot{\theta}}{\partial M}][Q_F] = [\varepsilon_{\ddot{\theta}M}][Q_F] \qquad (B-12)$$

The accelerations of a point on the rigid body result from the translational acceleration of the center of gravity and the linear acceleration due to pure rotations of the rigid body. The translational acceleration is obtained from Equations (B-6), (B-8), and (B-9) and is written as

$$\{\ddot{q}\} = \{F\}\frac{1}{M} + [Q_i][\varepsilon_{\ddot{\theta}M}][Q_F]\{F\} \qquad (B-13)$$

Equation (B-13) yields the rigid-body acceleration coefficient relating translational acceleration and force:

$$[\varepsilon_{\ddot{q}F}] \equiv [\partial\ddot{q}/\partial F] = [\frac{1}{M}] + [Q_i][\varepsilon_{\ddot{\theta}M}][Q_F] \qquad (B-14)$$

# LIST OF SYMBOLS

$a_{jki}$    i-th antiresonant frequency for response at j due to force at k - rad/sec

$A_{jki}$    modal acceleration of the i-th mode for response at j due to force at k - in./sec$^2$/lb

$C_{jk}$    jk-th influence coefficient - in./lb

$E_{jk}$    jk-th rigid body acceleration coefficient - in./sec$^2$

f    force - lb

g    structural damping coefficient

i    imaginary operator

$I_{jk}$    jk-th inertial coefficient - in./lb-sec$^2$

I    mass moment of inertia - lb-sec$^2$-in.

k    stiffness - lb/in.

K    stiffness - lb/in.

K    constant

M    mass - lb-sec$^2$/in.

m    mass - lb-sec$^2$/in.

N    number of modes

n    index

q    generalized coordinate

R    mobility residuals - in./lb-sec$^2$

S    defined in text

x    distance - in.

y    vibratory displacement - in.

$\ddot{y}$    vibratory acceleration - in./sec$^2$

Y    displacement mobility - in./lb

$\ddot{Y}$      acceleration mobility - in./(lb-sec$^2$)

z      distance - in.

Z      displacement impedance - lb/in.

$\ddot{Z}$      acceleration impedance - lb-sec$^2$/in.

$\phi_{ji}$      j-th element in the i-th normal mode

$\omega$      frequency - rad/sec

$\Omega_i$      i-th natural frequency - rad/sec

## BRACKETS

[ ]( ) matrix

[ ]      diagonal matrix

{ }      column or row vector

## SUPERSCRIPTS

R      real

I      imaginary

E      elastic modes

(j)      i-th trial

+      pseudoinverse

-1      inverse

T      transpose

# LIST OF SYMBOLS (Continued)

## SUBSCRIPTS

| | |
|---|---|
| i | modal index |
| m | modal index |
| M | modal index |
| (j) | subscript j constant |
| e | exciter station |
| R | restrained |
| F | free |

## OTHER INDICES

Capital letters under matrices indicate the number of rows and columns, respectively.